Master Thesis

Improvement of Thermal Stability of Ni Silicide on Heavily Doped N^+-Si

Supervisor

Professor Hiroshi Iwai

Iwai Laboratory

Department of Electronics and Applied Physics

Tokyo Institute of Technology

05M36269

Takashi Shiozawa

LIST OF CONTENT

Index 2

Chapter 1

INTRODUCTION 5

1 Background of this study 6

1.1 Low-Resistivity Materials for Nanoscale CMOS 9

1.2 Transition of Silicide Technology 11

1.3 Comparison of Silicide Materials 12

1.4 Purpose of This Study 16

Chapter 2

FABRICATION AND MEASUREMENTS 18

2 Flow of Experiments 19

2.1 Si Substrate Cleaning Process 19

2.2 UHV Sputtering System 20

2.3 Infrared Annealing Furnace 22

2.4 Four-point Probe Technique 24

2.5 Atomic Force Microscopy (AFM) 26

2.6 Scannin Electron Microscope (SEM) 27

2.7 X-ray Diffraction (XRD) 27

2.8 Auger Electron Spectroscopy 28

Chapter 3

EXPRIMENT RESULTS 30

3.1 Experimental results of pure Ni silicide 31

3.1.1 Fabrication process of Ni silicide 31

3.1.2 Characteristics of pure Ni silicide …..…................................... 33

3.2 Experimental results of Ni silicide with Al layer 40

3.2.1 Fabrication process of Ni silicide with Al layer 40

3.2.2 Characteristics of Ni silicide with Al layer 41

3.3 Experimental results of Ni silicide

with Al interlayer using TEG wafer 52

3.3.1 Fabrication process of Ni silicide

with Al interlayer on TEG wafer 52

3.3.2 Characteristics of Ni silicide

with Al layer on TEG wafer 53

3.4 Experimental results of Ni silicide

with other metal layers 60

3.4.1 Characteristics of Ni silicide with other metal layer 60

Chapter 4

CONCLUSIONS 60

4.1 Results of This Study 61

4.2 Future Issues 62

Acknowledgements 63

References 65

Chapter 1

INTRODUCTION

1. Background of This Study

About a half century ago, Brattain, Bardeen and Shockley succeeded in inventing the first transistor. Then, an integrated circuit (IC) is made by killby in 1948. After the invention of the IC, the number of transistors included in a chip have increased according to Moore's law and the semiconductor technologies have accomplished wonderful development.

CMOS (Complementary Metal Oxide Semiconductor) technology evolution in the past years has followed the path of device scaling for achieving density, speed, and power improvements. MOSFET (Metal Oxide Semiconductor Field-Effect Transistor) scaling was propelled by the rapid advancement of lithographic techniques for delineating fine lines of 1μm width and below.

In constant-field scaling, it was proposed that one can keep short-channel effects under control by scaling down the vertical dimensions (gate insulator thickness, junction depth, etc.) along with the horizontal dimensions, while also proportionally decreasing the applied voltages and increasing the substrate doping concentration (decreasing the depletion width). This is shown schematically in Fig. 1-1. The principle of constant-field scaling lies in scaling the device voltages and the device dimensions (both horizontal and vertical) by the same factor, $\kappa(>1)$, so that the electric field remains unchanged. This assures that the reliability of the scaled device is not worse than that of the original device.

Table 1-1 shows the scaling rules for various device parameters and circuit performance factors. The doping concentration must be increased by the scaling factor κ in order to keep Poisson's equation invariant with respect to scaling.

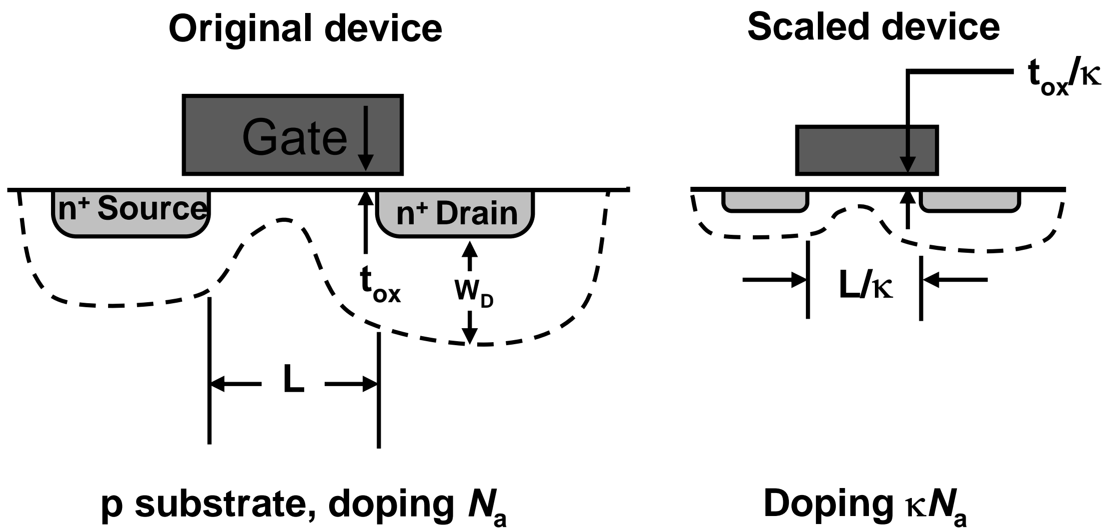

Fig. 1-1 Principles of MOSFET constant-electric-field scaling

Table 1-1 Scaling of MOSFET Device and Circuit Parameters

	MOSFET Device and Circuit Parameters	**Multiplicative Factor (κ>1)**
Scaling assumptions	Device dimensions(tox, L, W, χj)	1/κ
	Doping concentration (Na, Nd)	κ
	Voltage (V)	1/κ
Derived scaling behavior of device parameters	Elecric field (ξ)	1
	Carrier velocity (υ)	1
	Depletion –layer width (Wd)	1/κ
	Capacitance (C=εA/t)	1/κ
	Inversion-layer charge density (Qi)	1
	Current, drift (I)	1/κ
	CRchhannel resistance (Rch)	1
Capacitance behavior of circuit Power parameters	Circuit delay time (τ~CV/I)	1/κ
	Power dissipation per circuit (P~VI)	$1/\kappa^2$
	Power-delay product per circuit (Pτ)	$1/\kappa^3$
	Circuit density (∞ 1/A)	κ^2
	Power density (P/A)	1

The gate length of MOSFET came to be lower than 100nm since the year of 2000 and 32nm for the year of 2005 as shown in Fig. 1-2 according to the ITRS roadmap 2006 update[1]. With continuous scaling of device dimensions, IC performance is becoming more and more dependent upon the parasitic series resistance of the source/drain junctions and their contacts.

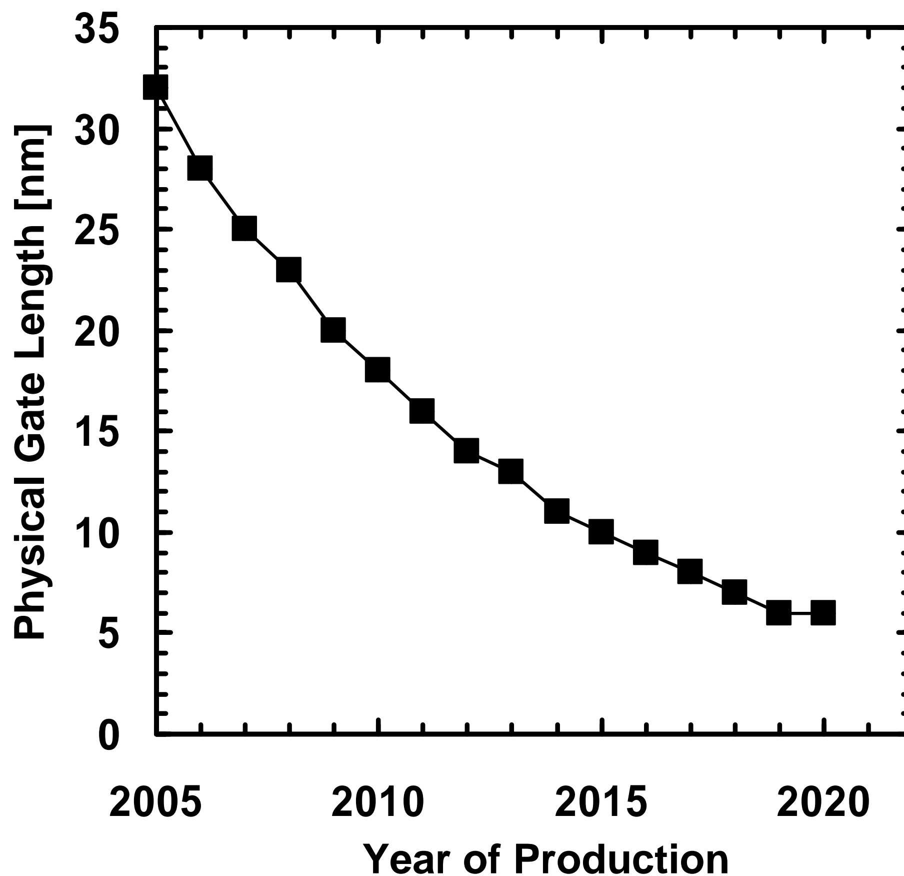

Fig.1-2 the International Technology Roadmap for Semiconductors (2006 update)

1.1 Low-Resistivity Materials for Nanoscale CMOS

The primary thrust of very large scale integration (VLSI) has resulted in devices that are smaller and faster and that consume less power. The continued evolution of smaller and smaller devices has aroused a renewed interest in the development of new metallization schemes for low-resistivity gates, interconnections, and ohmic contacts. This is interest in new metallization arose because as the device sizes are scaled down, the linewidth gets narrower and the sheet resistance contribution to the RC delay increases.

The conventional polysilicon whose sheet resistance is about 30 to 60 Ω/sq, is too high to be applied to modern VLSI. Aluminum, tungsten, and molybdenum are notable among the metals proposed for gate and interconnect metallization. The use of aluminum, however, requires all postgate processing of the devices to be limited to very low temperatures, preferably below $500^{o}C$. The use of the refractory metals tungsten and molybdenum requires complete passivation of these metals from oxidizing ambients, deposition by means that will not lead to unwanted traps in the gate oxide, and reliable etching of the metals for pattern generation. The uncertainties associated with the stability of these metal films have led to search for alternatives.

The silicides have attracted attention because of their low and metal-like resistivities and their high temperature stability. The use of silicides, with resistivity about one-tenth of the polysilicon, have greatly improved the speed of the circuits.

Scaling down the size of the device also means reduced junction depths, which can lead to contact problems. In particular, shallow junctions limit the use of aluminum due to its known penetration in silicon. Forming silicides in the contact windows by

reaction between the silicon substrate and a thin metal layer offers a possibility of forming contacts with lower contanct resistances.

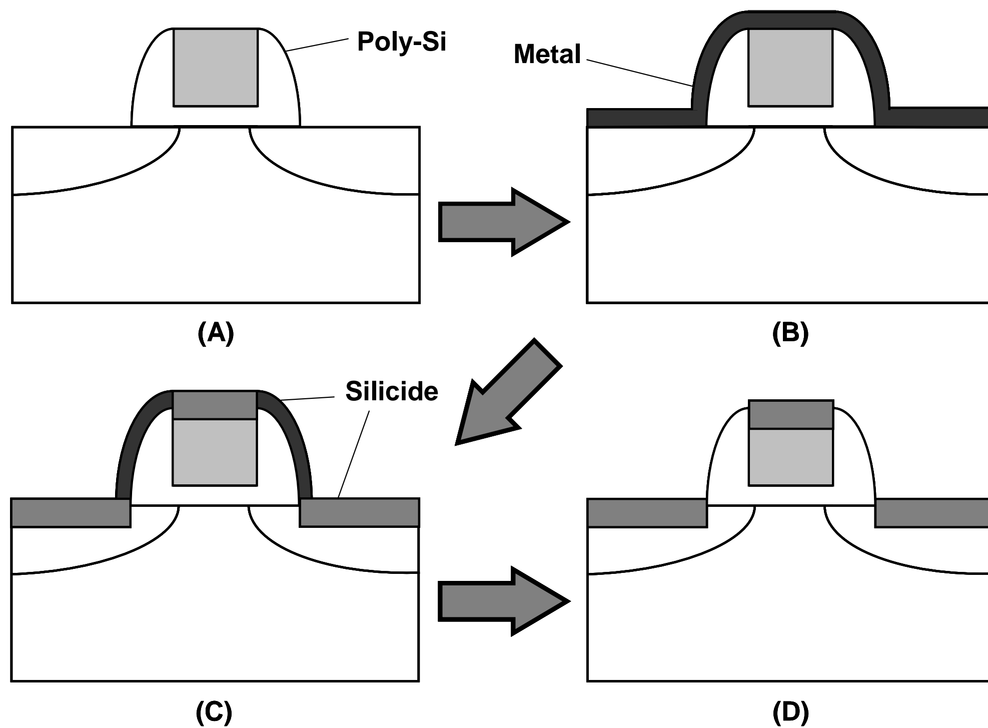

Fig.1- Self-Align Silicide (SALICIDE) Process.
(A) Conventional MOSFET before Metallization. (B) After Metal Deposition.
(C) After RTA for Silicidation. (D)After Selective Etching

1.2 Transition of Silicide Technology

Silicide was first introduced to LSI devices as a polycide (stacked silicide /poly Si gate electrode) as shown in Fig. 1-3. $MoSi_2$ polycide word line in 256 K DRAM in early 1980s was one of the first applications of polycide to LSI production. Then, WSi_2 polycide was popularly used for the gate electrode of logic LSIs from the middle of the 1980s because the sheet resistance of WSi_2 is smaller than that of $MoSi_2$. Salicide was popularly introduced into mass production using $TiSi_2$ in the early 1990s. $TiSi_2$ was selected as the material for salicide, because the sheet resistance is further smaller than WSi_2. However, $TiSi_2$ was eventually found to be a relatively difficult material to treat depending on thermal process. For example, sheet resistance of $TiSi_2$ often increases by the agglomeration of the silicide film during high temperature thermal process of the CMOS fabrication. Thus, $TiSi_2$ has been eventually replaced by $CoSi_2$ from the late 1990s making the process more suitable towards deep-sub micron CMOS [3]. In December 1991, NiSi-salicide was proposed for the first time with the demonstration of nice characteristics of a 0.4-mm NiSi salicided CMOS [2]. Moreover, NiSi is lower resistance and consumes less Si than that of $CoSi_2$. Now NiSi is considered to be a promising silicide material for nanoscale CMOS. The progress of silicide technologies summarized as Fig. 1-3[3].

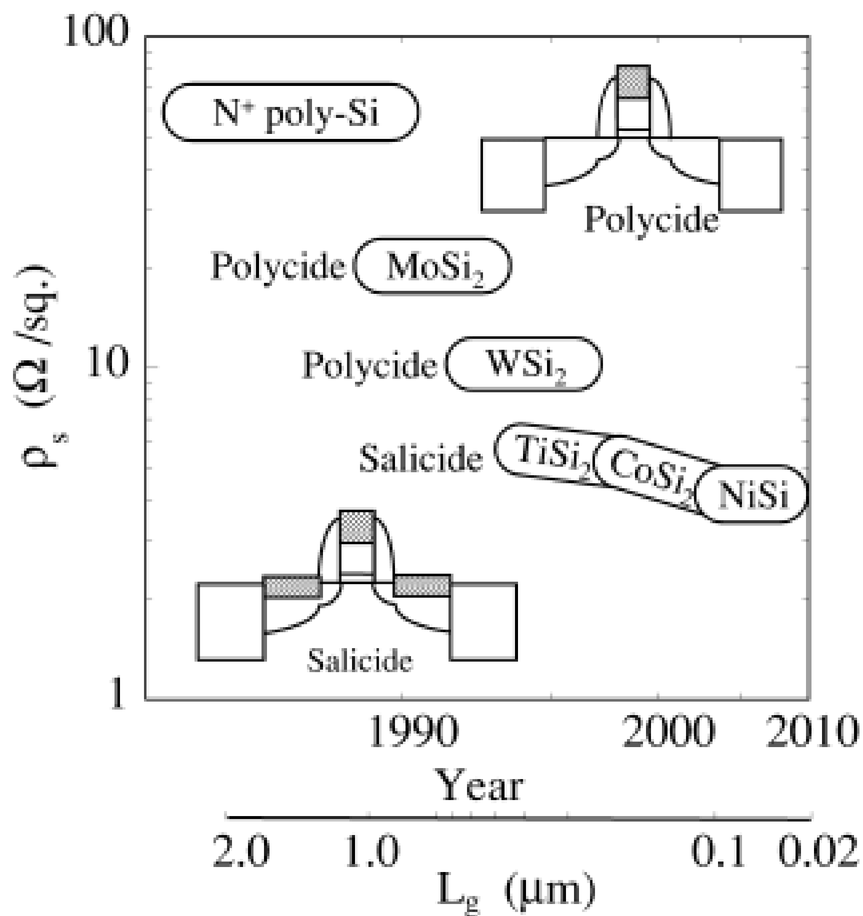

Fig. 1-3 Progress of silicate materials

1.3 Comparison of Silicide Materials

The main driver for the continuous advancement in VLSI has been the search for electronic circuits of higher performance and lower cost. In particular, the speed of an electronic circuit is one of the major concerns. For this purpose of reaching higher speed, metal silicates have been utilized for contact metallization and local wiring. The choice of metal silicates in LSIs technology is quite natural, because they meet the basic requirements: low specific resistively, low contact resistively to both types of LSIs, high thermal stability, and excellent process compatibility with standard Si technology.

Today, metal silicides are an inseparable part of an electronic device. Here are some comparisons about silicide materials. Fig. 1-4 shows the dependence of sheet resistance on line width for various silicide materials. Ni silicide possesses not only the lowest sheet resistance but also the best width independence among $TiSi_2$(Conventional process), $TiSi_2$(Pre-amorphization) and $CoSi_2$ as well.

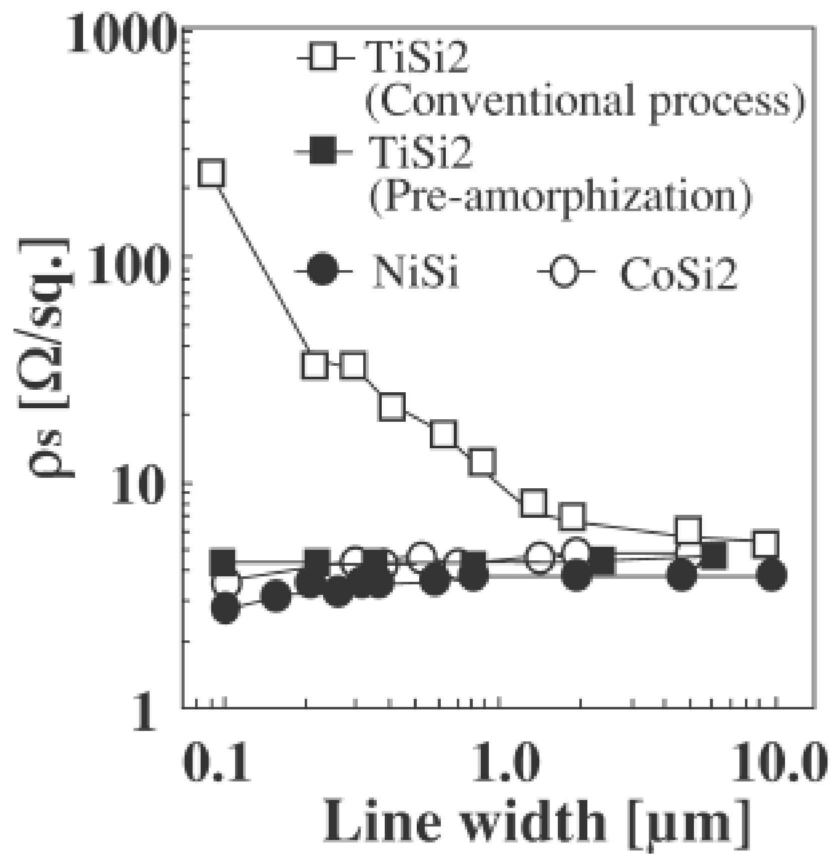

Fig. 1-4 Dependence of sheet resistance on line width for various silicide materials

Ni silicide shows the lowest sheet resistance also can be confirmed from table 1-2. However, at higher temperature or more than 700°C, Ni silicide begins to transform to $NiSi_2$ whose resistivity is 2 or 3 times as high as that of NiSi. In other words, Ni silicide is poor at thermal stability. Table 1-3 indicates some physical properties of Ti, Co, Ni silicide.

TABLE 1-2 Parameters for Silicide Processing Using Ti, Co or Ni[4]

Silicide	T_f(^{o}C)	ρ (μΩcm)	Φ_{Bn} (eV)[d)]	DDS[e)]
C49 $TiSi_2$	350-700[a)]	60-80		Si
C54 $TiSi_2$	700[b)]	15-20	0.60	Si
Co_2Si	350	110		Co
CoSi	375	147	0.68	Si
$CoSi_2$	500	15-20	0.64	Co
NiSi	250-400	10.5-15	0.65	Ni
$NiSi_2$	700-800[b)]	34	0.66	Ni

a) Upper limit dependingon thickness, feature size and doping level.
b) Depending on thockness, feature size and doping level.
c) When formed from NiSi through anucleation controlled process.
d) Φ_{Bn}: Schottky barrier height to n-type Si.
e) DDS – Dominant diffusion species duaring formation.

Metal	Temperature 1st RTP (^{o}C)	Phase to form sfter 1st RTP	Wet selective etching	Temperature 2nd RTP (^{o}C)	Phase to form after 2nd RTP
Ti	650-730	C49 $TiSi_2$	H_2SO_4:H_2O_2 + NH_4OH:H_2O_2;H_2O	>850	C54 $TiSi_2$
Co	400-600	CoSi	H_2SO_4:H_2O_2	>700	$CoSi_2$
Ni	400-550	NiSi	H_2SO_4:H_2O_2	-	-

TABLE 1-3 Some Physical Properties of Ti, Co and Ni Silicides

Metal	Silicide phase	Crystal structure	T_m (K)	Lattice constant ()		
				A	B	C
Ti	Ti_3Si	Tetragonal	1440	10.196	-	5.097
	Ti_5Si_3	Hexagonal	2400	7.429	-	5.139
	Ti_5Si_4	Tetragonal	2190	6.702	-	12.174
	TiSi	Orthorhombic	1840	3.618	6.492	4.973
	C49 $TiSi_2$	Based-centered orthorhombic		3.562	13.531	3.55
	C54 $TiSi_2$	Faced-centered orthorhombic	1750	8.2687	8.5534	4.7913
Co	Co_3Si	Hexagonal	1480	4.976	-	4.069
	Co_2Si	Orthorhombic	1600	4.918	3.738	7.109
	CoSi	Cubic	1700	4.4443	-	-
	$CoSi_2$	Cubic	1600	5.365	-	-
Ni	Ni_3Si	Cubic	1440	3.504	-	-
	Ni_2Si	Orthorhombic	1580	5	3.73	7.04
	NiSi	Cubic		4.446	-	-
	NiSi	Orthorhombic	1265	5.18	3.34	5.62
	$NiSi_2$	Cubic	1298	5.406	-	-
Si	Si	Cubic	1683	5.306	-	-

1.4 Purpose of This Study

As mentioned in section 1.3, the thermal stability of Ni silicide is very poor. Compared with other silicide materials as shown in Fig. 1-5, Ni silicide is so sensible to heat that its degradation temperature is only 500-600°C. Ni silicide forms at about 350°C and turns to be a high resistance material called $NiSi_2$ at the temperature of about 700 ^{o}C on P-type Si. While the thermal stability of Ni silicide on heavily doped N^+ substrates with As concentration of ~10^{20}/cm^3, whose density is expected for the 45nm node exhibited considerable degradation compared with that on the P^+ substrates to mention it later. Thus, the purpose of this study is to find out the method to improve the thermal stability of Ni silicide on heavily doped N^+ Si with maintaining quality of thermal stability the case its method is adopted to P^+ heavily doped Si.

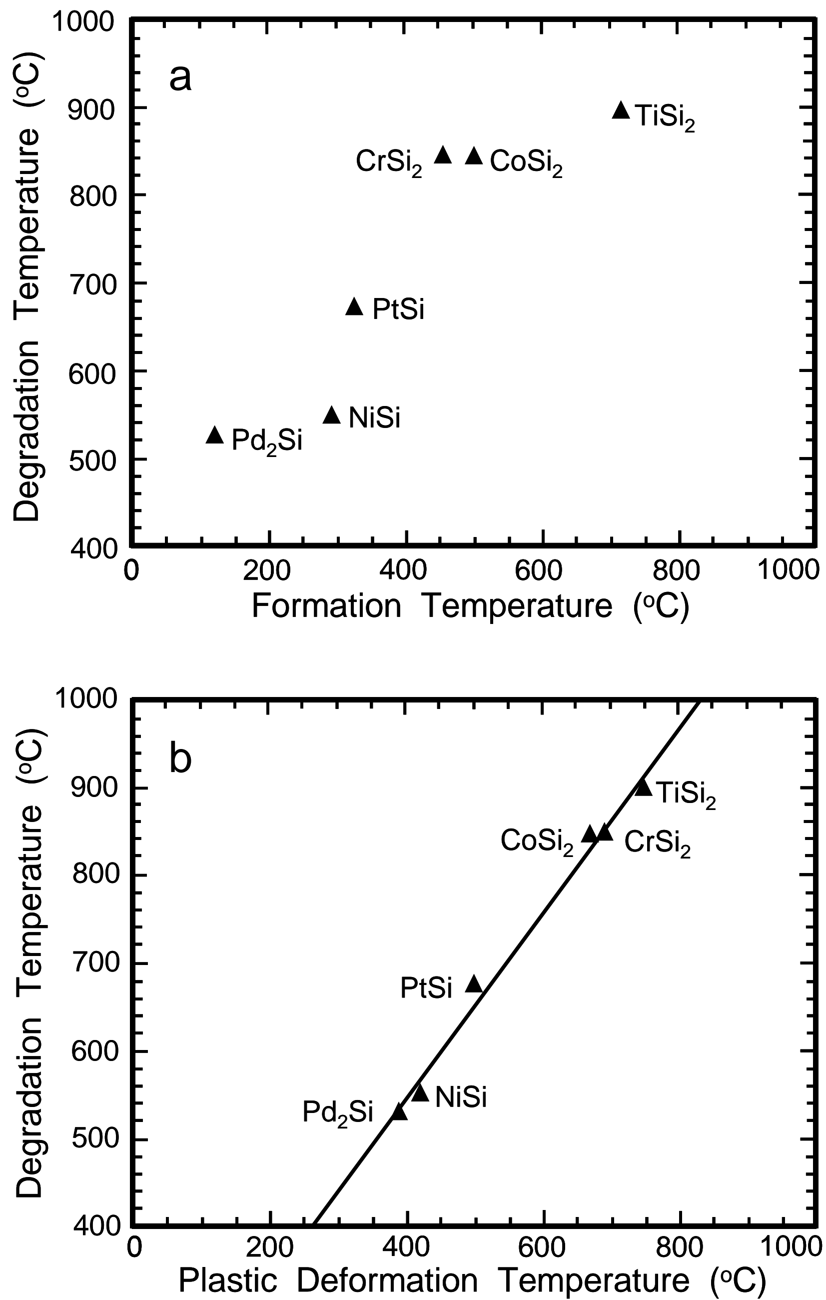

Fig.1-5 Silicide degradation temperature vs.(a) silicide formation temperature and (b) deformation temperature for six silicides. [5]

Chapter 2

FABRICATION AND MEASUREMENTS

2 Flow of Experiments

In this chapter, experiment instruments which were used in this study were introduced. Before these introductions, flow of experiments was presented in brief.

N-type (100)Si substrates with As concentration of ~$10^{20}/cm^3$, whose density is expected for the 45nm node, were used in this study.

After Si substrate was cleaned by SPM and diluted HF, film structures M/Ni/Si, Ni/M/Si, Ni/M/Ni/Si(Here M is a metal additive except Ni.) and Ni/Si were deposited on Si (100) substrates by using an UHV-sputtering system after substrate cleaning process. Then these samples were annealed in forming gas (N_2:H_2=97:3) ambient using a rapid thermal annealing (abbreviated as RTA) system. Sheet resistance of the silicide layers was measured by the four point probe method. Structures of the layers were observed by AFM, XRD, AES etc.

2.1 Si Substrate Cleaning Process

At first, high quality thin films require ultra clean Si surface without particle contamination, metal contamination, organic contamination, ionic contamination, water absorption, native oxide and atomic scale roughness.

One of the most important chemicals used in Si substrate cleaning is DI (de-ionized) water. DI water is highly purified and filtered to remove all traces of ionic, particulate, and bacterial contamination. The theoretical resistivity of pure water is 18.25 MΩcm at 25°C. Ultra-pure water (UPW) system used in this study provided UPW of more than 18.2 MΩcm at resistivity, fewer than 1 colony of bacteria per milliliter and fewer than 1 particle (fΦ0.1μm) per milliliter.

In this study, the Si substrate was cleaned on a basis of RCA cleaning process,

which was proposed by W. Kern et al. But some steps were reduced. The flow of the Si clean process was shown as Fig.2.1. The first step, which use a solution of sulfuric acid (H_2SO_4) / hydrogen peroxide (H_2O_2) (H_2SO_4: H_2O_2=4:1), was performed to remove any organic material and metallic impurities. After that, the native or chemical oxide was removed by diluted hydrofluoric acid (HF:H_2O=1:99). Then the cleaned wafer was dipped in DI water. Finally, the cleaned Si substrate was loaded to chamber to deposit as soon as it was dried by air gun.

2.2 UHV-Sputtering System

After cleaned by chemicals, film structures such as M/Ni/Si, Ni/M/Si (Here M is a metal additive except Ni.) and Ni/Si were formed by an UHV-sputtering system.

Sputtering is one of the vacuum processes used to deposit ultra thin films on substrates. It is performed by applying a high voltage across a low-pressure gas (usually argon at about 5 millitorr)to create a "plasma," which consists of electrons and gas ions in a high-energy state. Then the energized plasma ions strike a "target," composed of the desired coating material, and cause atoms from that target to be ejected with enough energy to travel to, and bond with the substrate.

An UHV-sputtering system is used for thin film formations of electronic devices, for experiments of GMR, and for creating new materials of high temperature superconductors. In this study, UHV Multi Target Sputtering System ES-350SU shown as Fig. 2-2 was conducted. The rotating function of target positioning is developed, enabling this system to sputter 5 targets by means of DC & RF power sources by using a single electrode. The substrate holder can be rotated and its speed can be selected. As for other details, Table 2-1 is attached for reference.

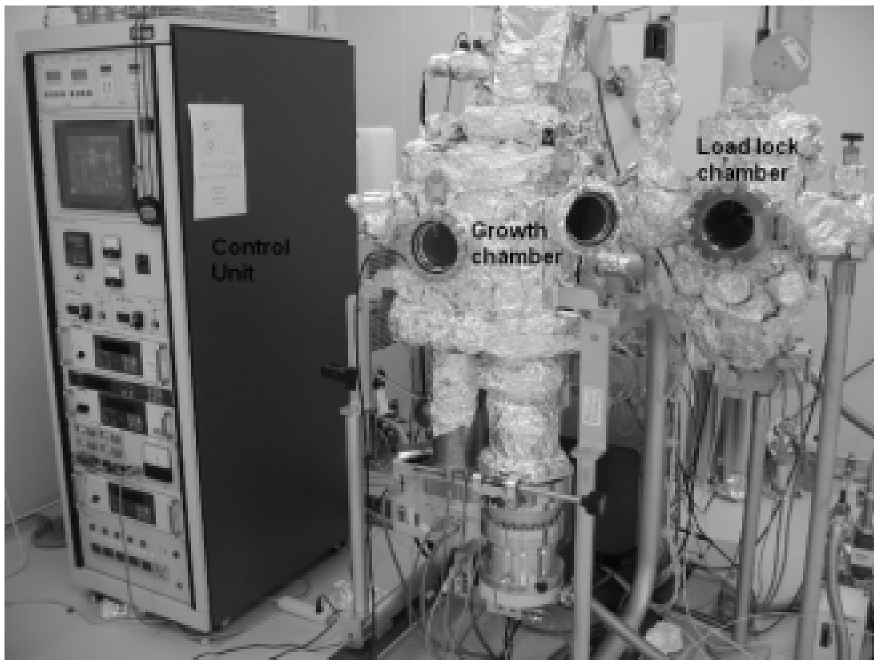

Fig. 2-2 Photo of UHV Multi Target Sputtering System ES-350SU

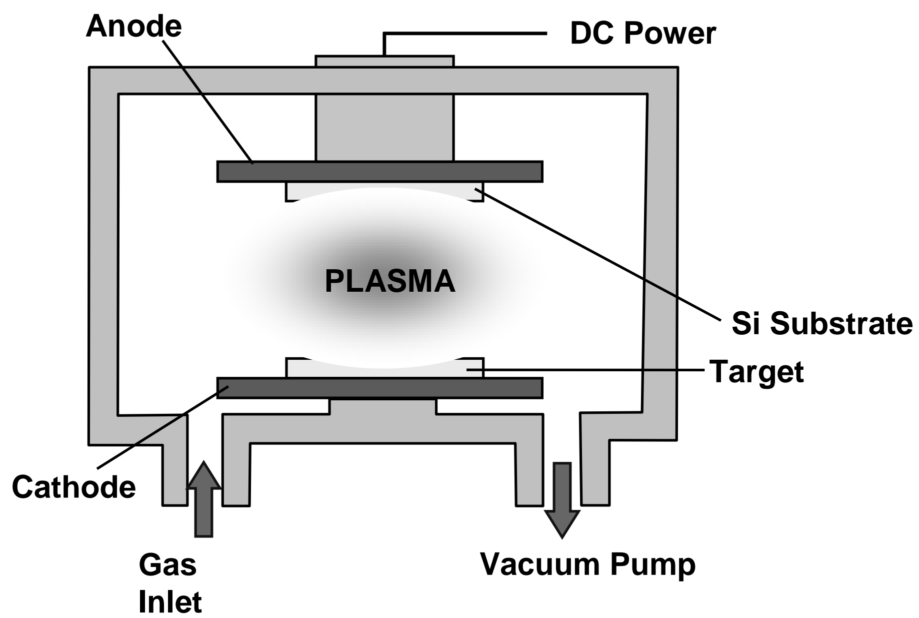

Fig. 2-3 structure of UHV sputtering system

Table 2-1 Specifications for UHV Multi Target Sputtering System ES-350SU

Growth chamber	1. Ultimate pressure	1.5 x 10^{-6}Pa
	2. Substrate size	2 inch in diameter
	3. Heating temperature	600ºC
	4. Heater type	Lamp type heater
	5. Target	3 inch x 5 pieces (motor-driven)
Load lock chamber	6. Vacuum pumps	TMP 500L/sec and RP 250L/min
	7.Ultimate pressure	6.6 x 10^{-5}Pa
	8. Vacuum pumps	TMP60L/sec and RP90L/min
	9. Substrate holder with cooling function / Substrate holder with heating function /Cleaning function / Radical beam source	

2.3 Infrared Annealing Furnace

After formation from UHV sputtering system, thin films of Ni/Si, Ni/M/Si, M/Ni/Si were moved to annealing furnace to hold thermal process.

In order to obtain high quality films, annealing process after deposition is required. The annealing after deposition is considered to bring the suppression of leakage current because of the defects in the films and surface roughness. In this study, thermal process leads to the reaction of Ni with Si.

The equipment for annealing used in this investigation was QHC-P610CP (ULVAC RIKO Co. Ltd). Fig. 2-4 is the photo of the infrared annealing furnace, whose schematic illustration was shown as Fig. 2-5. The annealing was performed by six infrared lamps surrounding the sample stage which were made of carbon and coated by SiC. The heating temperature was controlled by thermocouple feedback.

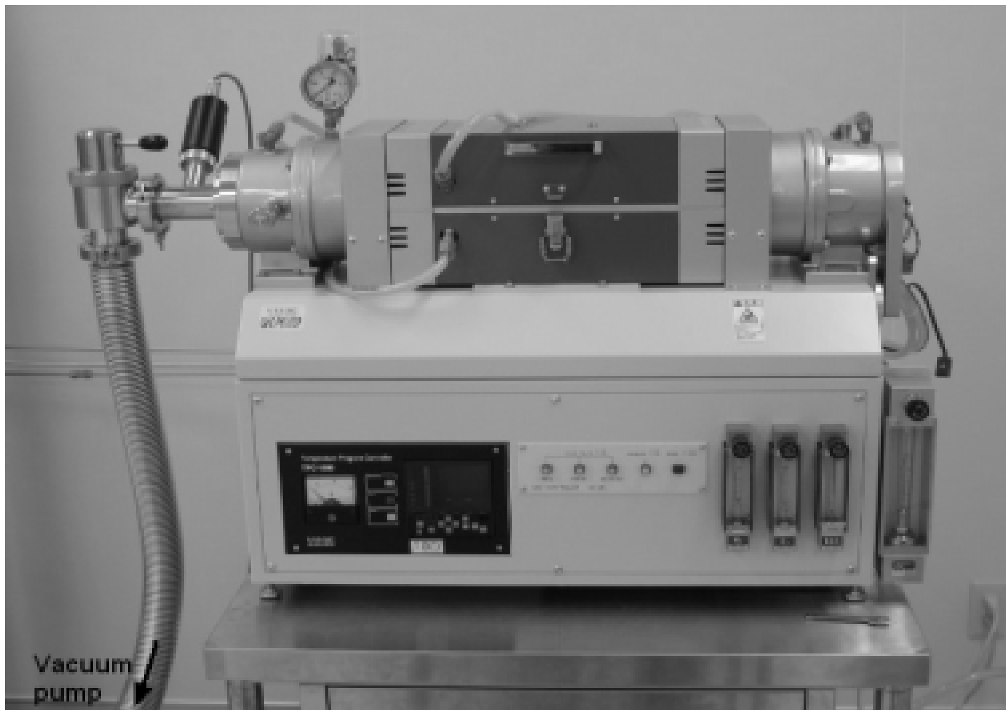

Fig. 2-4 Photo of infrared annealing furnace

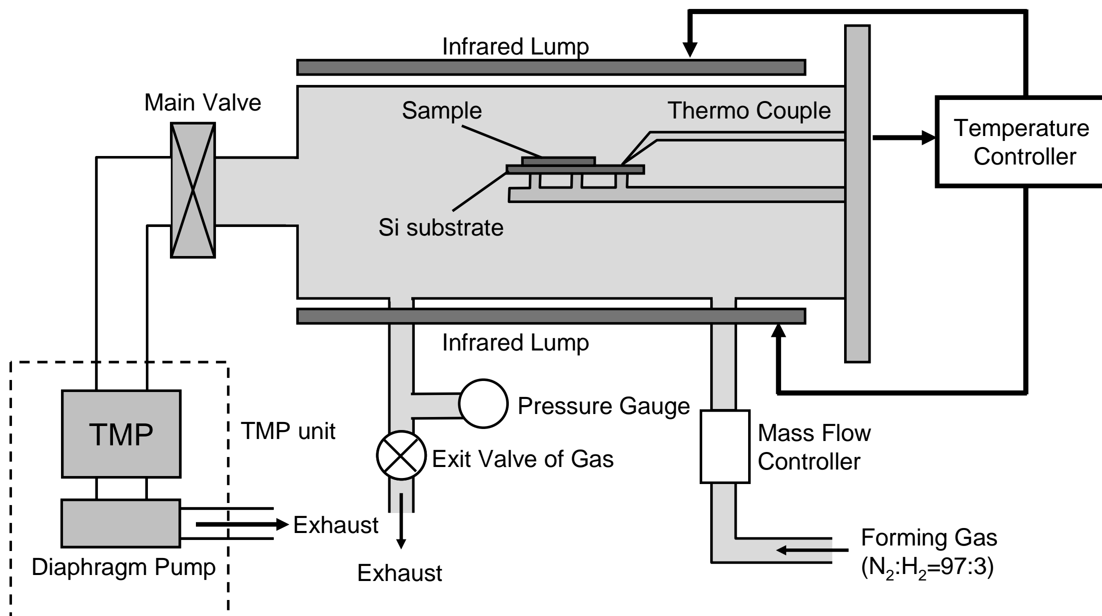

Fig. 2-5 schematic image of infrared annealing furnace

2.4 Four-point Probe Technique

The sheet resistance of Ni silicide was measured by four-point probe technique. The phase of Ni can be ascertained according to the sheet resistance of Ni silicide thin film, because the sheet resistance of $NiSi_2$ is greatly different from that of Ni monosilicide (NiSi) or other phase such as Ni_2Si.

The four-point probe technique is one of the most common methods for measuring the semiconductor resistivity because two-point probe method is difficult to interpret. The sheet resistance is calculated form potential difference between inside 2 terminals (between B probe and C probe) after applying the current between outside 2 terminals (between A probe and D probe) as shown in Fig.2-6. The resistance by two-probe technique is higher than accurate resistance because it includes the contact resistance (R_C) between metal probe and semiconductor surface and spreading resistance (R_{SP}) of each probe. Neither R_C nor R_{SP} can be accurately calculated so that semiconductor resistance (R_S) cannot be accurately extracted from the measured resistance. On the other hand, four-probe technique can neglect these parasitic resistances because the current value which flows between terminals is very small and potential drop can be disregarded. In this study, sheet resistance was measured by four-probe technique.

For an arbitrarily shaped sample the sheet resistance (ρ_{sh}) is given by

$$\rho_{sh} = V/I * CF \qquad (2\text{-}1)$$

where *CF* is correction factor that depends on the sample geometry. If the distance among probes (s; in this study, s=1 mm) is greatly shorter than the width of a sample (d), *CF* equals to $\pi/\ln(2)=4.53$.

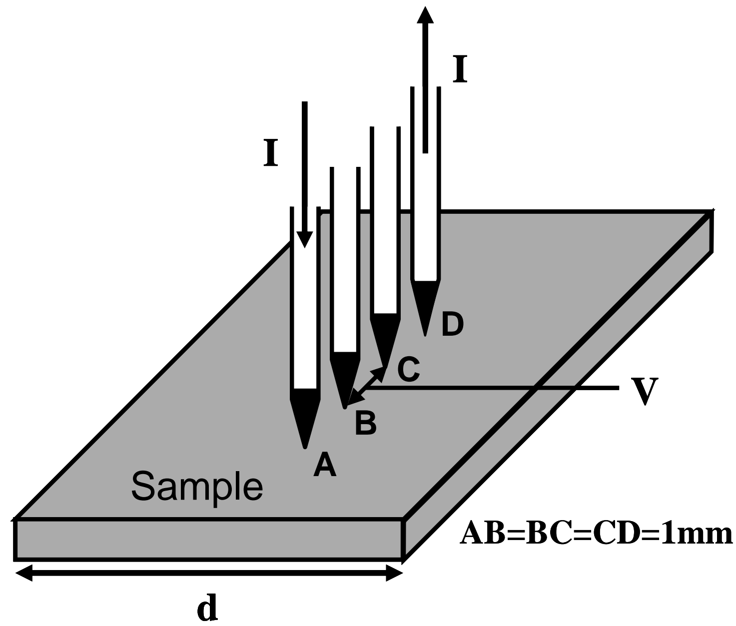

Fig. 2-6 illustration of four point probe system

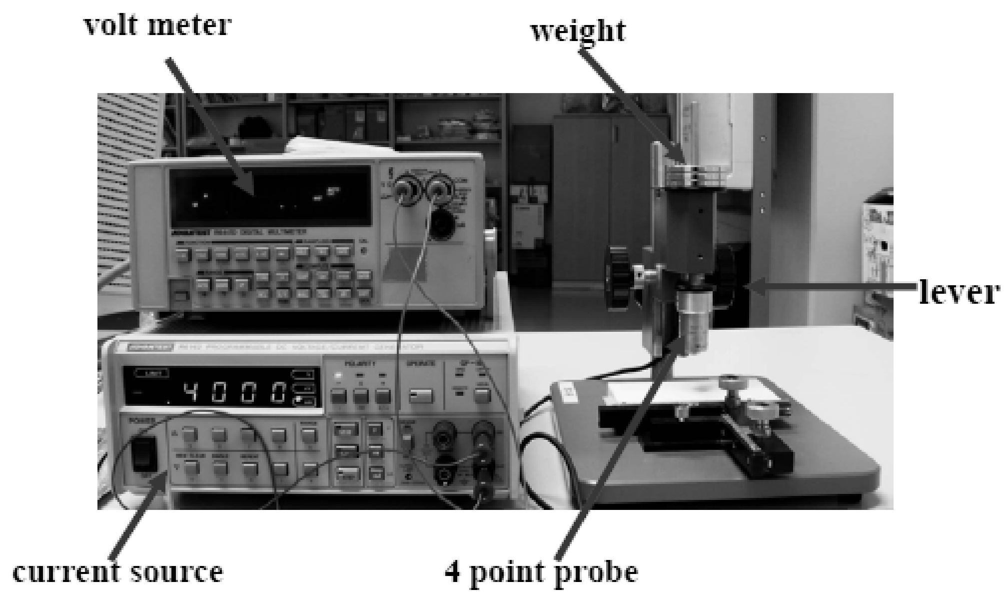

Fig. 2-7 Photo of four point probe system

2.5 Atomic Force Microscopy (AFM)

AFM enables to measure surface morphology by utilizing force between atoms and approached tip. The roughness of sample surface is observed precisely by measurement of x-y plane and z. Fig. 2-7 shows the principle of AFM.

The basic objective of the operation of the AFM is to measure the forces (at the atomic level) between a sharp probing tip (which is attached to a cantilever spring) and a sample surface. Images are taken by scanning the sample relative to the probing tip and measuring the deflection of the cantilever as a function of lateral position. Typical spring constants are between 0.001 to 100 N/m andmotions from microns to ~ 0.1Å are measured by the deflection sensor. Typical forces between tip and sample range from 10^{-11} to 10^{-6}N. For comparison the interaction between two covalently bonded atoms is of the order of 10^{-9}N at separations of ~1Å.Therefore, non-destructive imaging is possible with these small forces Compared with Scanning Electron Microscope, AFM provides extraordinary topographic contrast direct height measurements and unobscured views of surface features.

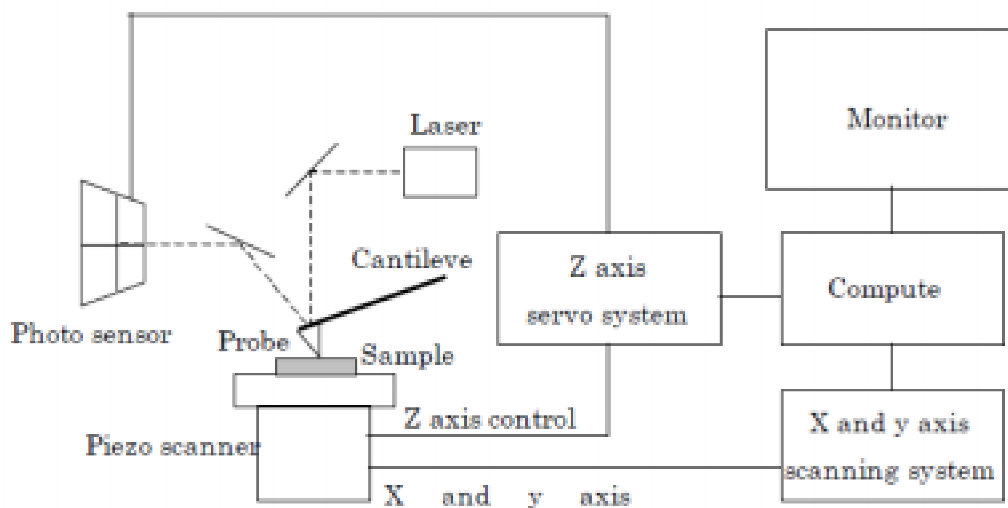

Fig. 2-7 Principle of AFM

2.6 Scanning Electron Microscope (SEM)

The Scanning Electron Microscope (SEM) is a microscope that uses electrons rather than light to form an image. There are many advantages to using the SEM instead of a light microscope. The SEM has a large depth of field, which allows a large amount of the sample to be in focus at one time. The SEM also produces images of high resolution, which means that closely spaced features can be examined at a high magnification. Preparation of the samples is relatively easy since most SEMs require the sample to be conductive. The combination of higher magnification, larger depth of focus, greater resolution, and ease of sample observation makes the SEM one of the most heavily used instruments in research areas today. The SEM uses electrons instead of light to form an image. A beam of electrons is produced at the top of the microscope by heating of a metallic filament. The electron beam follows a vertical path through the column of the microscope. It makes its way through electromagnetic lenses which focus and direct the beam down towards the sample. Once it hits the sample, other electrons (backscattered or secondary) are ejected from the sample. Detectors collect the secondary or backscattered electrons, and convert them to a signal that is sent to a viewing screen similar to the one in an ordinary television, producing an image.

2.7 X-ray Diffraction (XRD)

X-ray Diffraction (XRD) is a powerful non-destructive technique for characterizing crystalline materials. It provides information on structures, phases, preferred crystal orientations (texture) and other structural parameters such as average grain size, crystallinity, strain and crystal defects. X-ray diffraction peaks are produced

by constructive interference of monochromatic beam scattered from each set of lattice planes at specific angles. The peak intensities are determined by the atomic decoration within the lattice planes. Consequently, the X-ray diffraction pattern is the fingerprint of periodic atomic arrangements in a given material. An on-line search of a standard database for X-ray powder diffraction pattern enables quick phase identification for a large variety of crystalline samples.

2.8 Auger Electron Spectroscopy

Auger Electron Spectroscopy (*Auger spectroscopy* or AES) is a surface specific technique utilizing the emission of low energy electrons in the *Auger process* and is one of the most commonly employed surface analytical techniques for determining the composition of the surface layers of a sample. The Auger electron is a secondary electron discharged to a vacuum by a process shown for Fig.2-8. The Auger effect occurs because the incident electrons can remove a core state electron from a surface atom. This core state can be filled by an outer shell electron from the same atom, in which case the electron moves to a lower energy state, and the energy associated with the transition is the difference in orbital energies. This energy must be released in some fashion. In some cases this energy is imparted to a second outer shell electron, which then is ejected from the atom. The characteristic energy of this ejected electron is

$$E_{Core\ State} = E_{S1} + E_{S2}$$

where S1 and S2 are the outer shell states. Because these orbital energies are determined by the element of the atom, the composition of a surface can be determined. When a primary electron beam was irradiated on the sample surface, an incidence electron activates an electron of an inner shell of a sample atom, and a cavity is made.

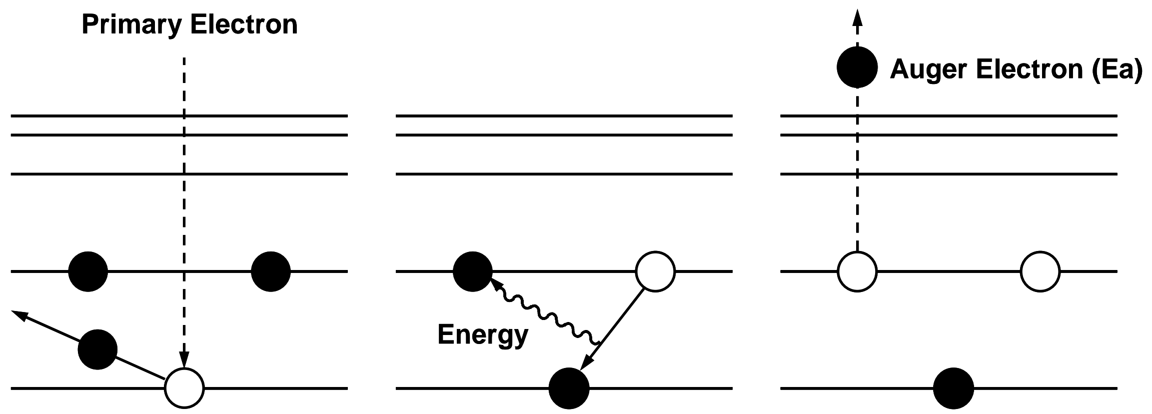

Fig. 2-8 Principle of AES

Chapter 3

EXPERIMENT RESULTS

3.1 Experimental results of pure Ni silicide

In this section, pure Ni silicide was studied to understand its characteristics and improvement its poor thermal stability. Four kinds of pure Ni silicides (P-type or N-type, heavily doped or lightly doped) were systemically investigated.

3.1.1 Fabrication process of Ni silicide.

Fabrication process of Ni silicide is showed Fig.3-1. Cleaning process was as follows. Si wafers were dipped into UPW first for 10 minuets. Secondary, conventional chemical cleaning using SPM (H_2SO_4:H_2O_2=4:1) solution was performed. And then they were dipped into UPW again for 10 minuets. After that they were dipped hydrofluoric acid (HF) for 5 minuets. Finally, the cleaned wafer was rinsed in UPW and loaded to suppurating system immediately. Then Ni film was deposited in-situ on Si(100) wafer. After deposition of Ni, rapid thermal annealing was carried out in forming gas ambient. Fig.3-2 shows temperature profile of RTA that temperature was raised to 150°C in first 1 minute, and kept 150°C next 3 minutes to stabilize and do condition fairly.

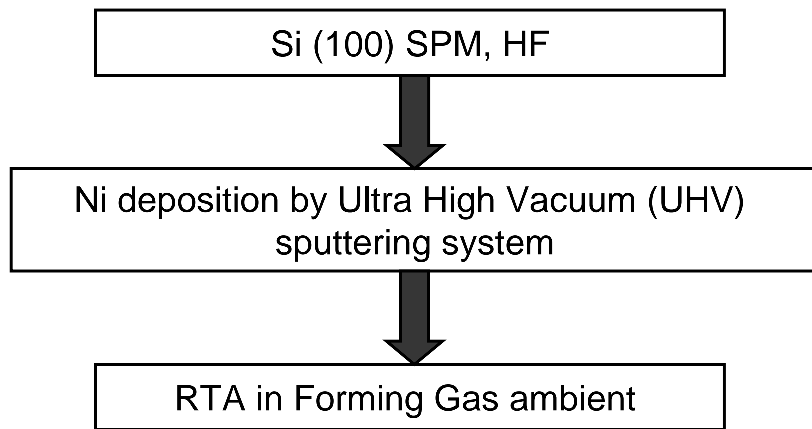

Fig.3-1 Fabrication process of pure Ni silicide.

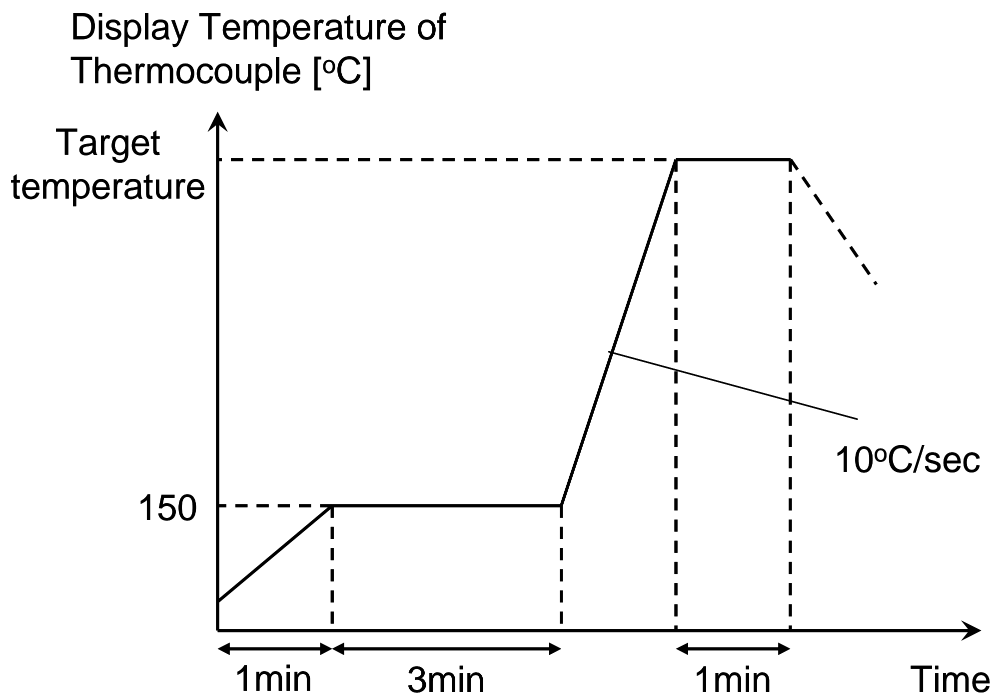

Fig.3.2 Pattern diagrams of Rapid Thermal Anneal (RTA)

3.1.2 Characteristics of pure Ni silicide.

At first, pure Ni silicide (Ni deposition:12nm) was investigated on heavily doped P^+ (B implanted) and N^+ (As implanted) substrates. The results were shown in Fig.3-3. On P^+ substrate, Ni silicide's phase of NiSi(Ni mono silicide) was formed in the temperature region from 300 to 700°C. NiSi phase is lowest and constant sheet resistance phase. Over 700°C, the phase transition from NiSi to $NiSi_2$ occurred and sheet resistance increased. Then up to 775°C silicide's phase completely transited to $NiSi_2$ and sheet resistance became constant with a high value. When temperature became higher than 925°C, hard agglomeration occurred and sheet resistance increased drastically. On the other hand, on N^+ substrate, Ni silicide shows low sheet resistance same as P^+ substrate at comparatively low temperature (400 to 600°C). But over 600°C, sheet resistance increased drastically like Ni silicide on P^+ substrate over 925°C. Fig.3-4 shows Ni silicide's (Ni deposition:12nm) surface roughness measured by AFM compared to sheet resistance. The surface roughness increased corresponding to sheet resistance. It means that the hard agglomeration occurred over 600°C. It can be seen from surface morphologies of Ni silicide layers measured by AFM and SEM. Fig.3-5 and Fig.3-6 shows pure surface morphology of pure Ni siliside formed on N^+ substrate at 600°C and 700°C respectively. Smooth surface was observed at 600°C silicidation. However, hard agglomeration was observed at 700°C silicideation. A similar result was provided from SEM images as shown Fig.3-7 (a) 600°C (b) 700°C.

Four kinds of pure Ni silicides (P-type or N-type, heavily doped or lightly doped) were systemically investigated successively as shown Fig.3-8. The results was divided into two groups, one is that the hard agglomeration occurred with transition from NiSi to $NiSi_2$, the other is that the hard agglomeration occurred after finishing transformation

from NiSi to $NiSi_2$ completely. In other words, as for the former, the agglomeration region come after the NiSi region, and the later has another region such as the $NiSi_2$ region between the NiSi region and the agglomeration region. (Heavily doped N^+ Si belongs to former and the others belong to later) It is seen from Fig.3-8 that what is nearer to Ni silicide on Heavily doped p-type Si has better thermal stability.

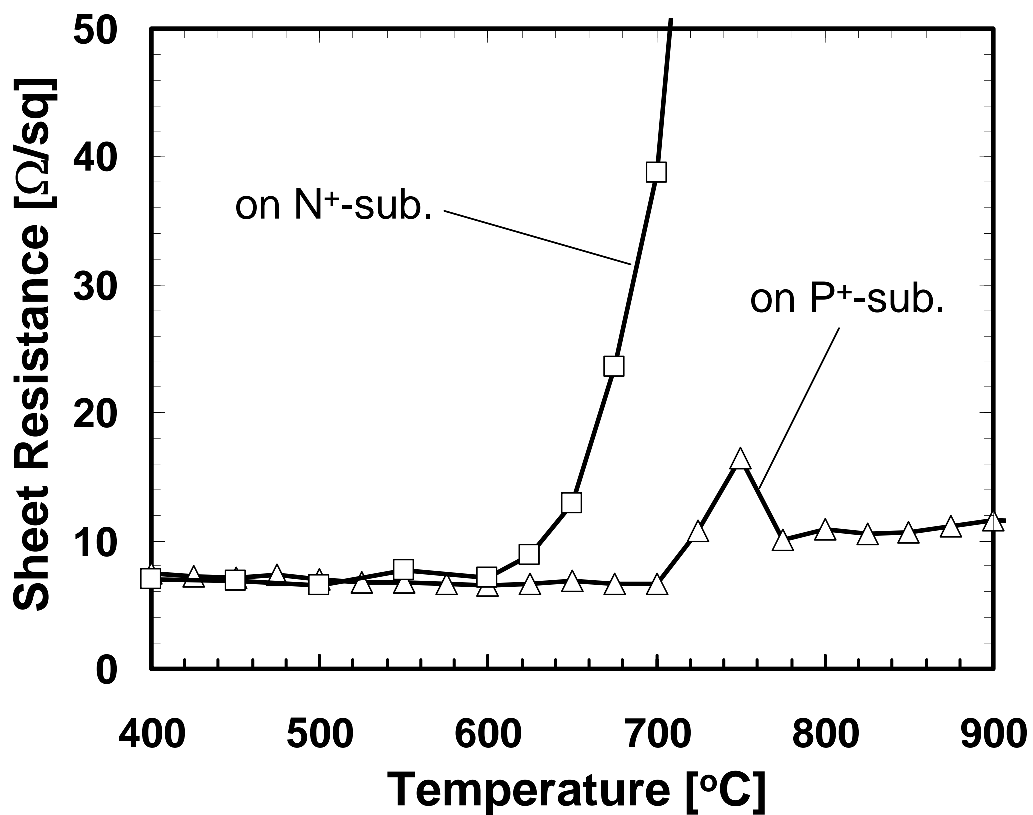

Fig.3-3 Transformation curves for Ni silicide on heavily doped N^+ and P^+ Si substrates (Ni deposition:12nm).

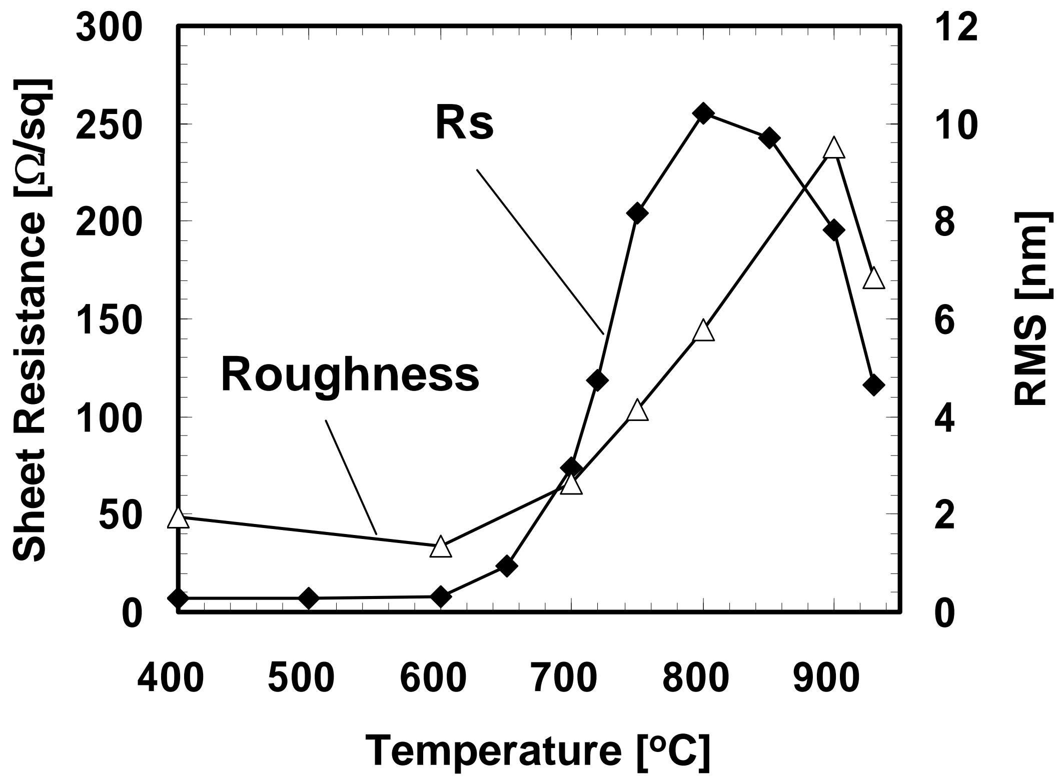

Fig.3-4 Surface roughness of Ni silicide on heavily doped N^{+}-Si as a function of RTA temperature.

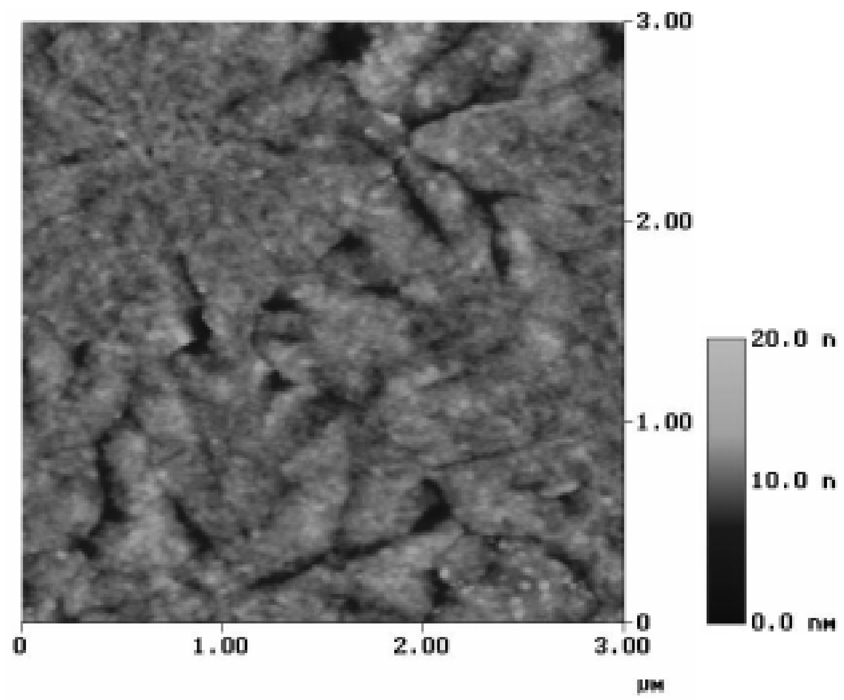

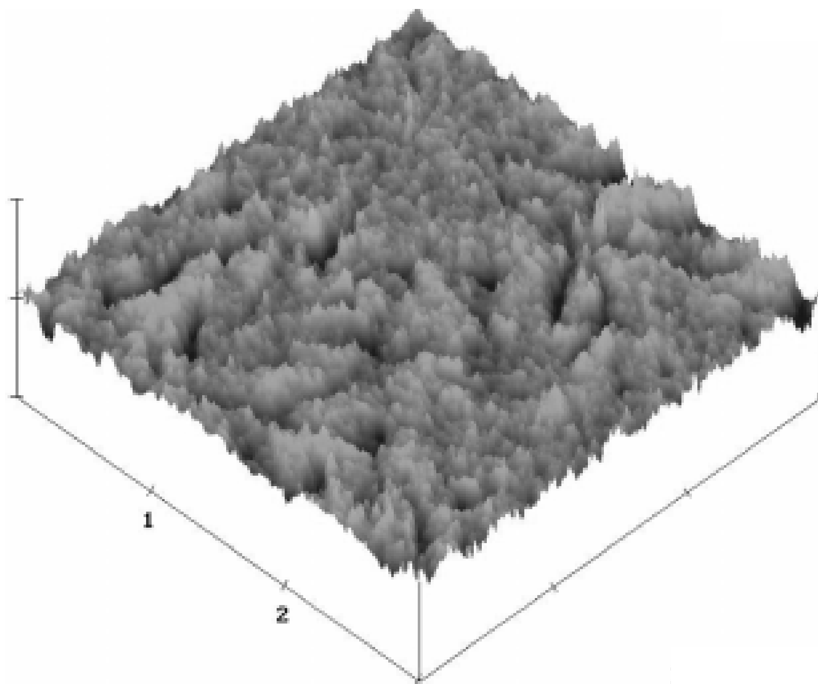

Fig.3-5 AFM images of pure Ni silicide at 600°C

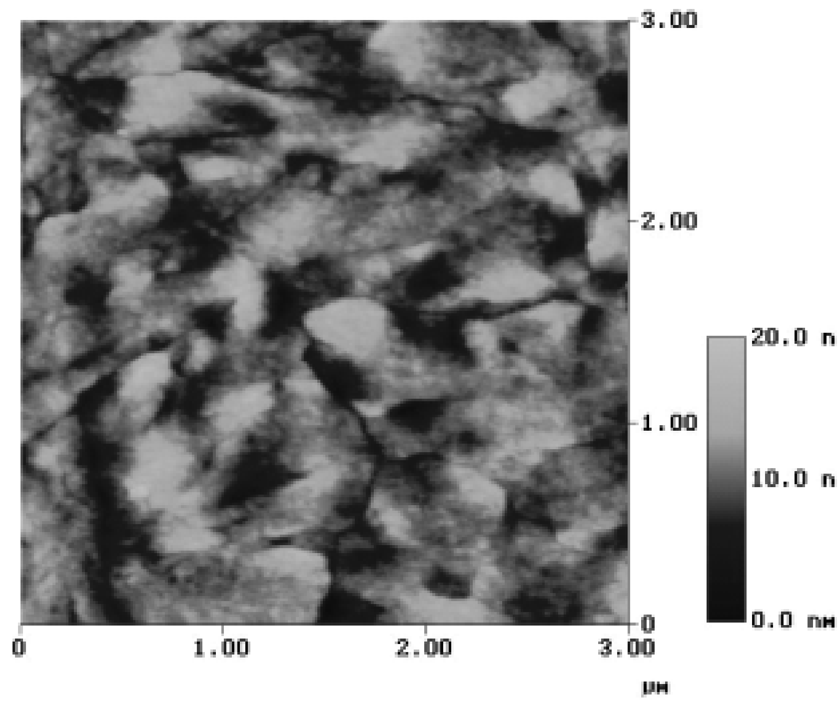

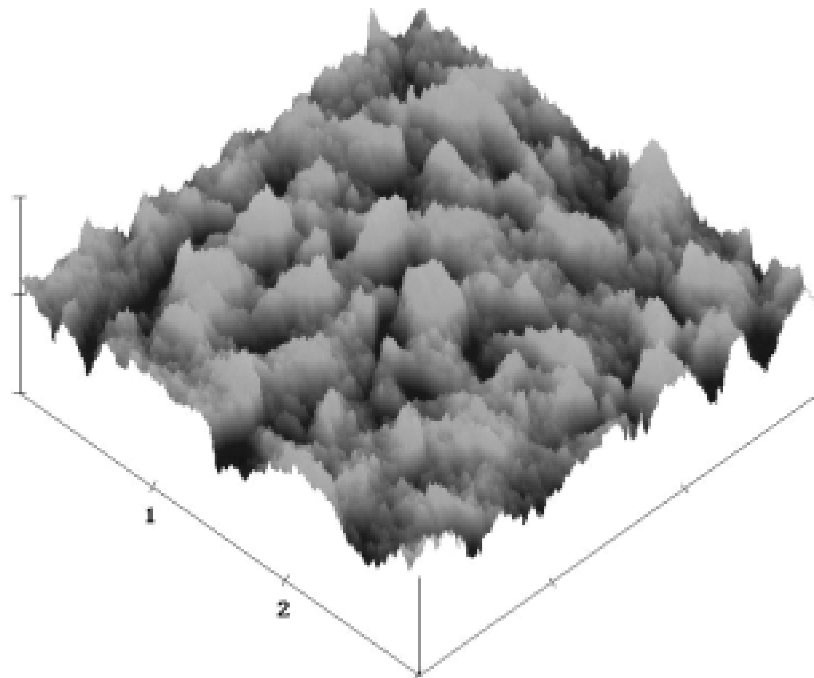

Fig.3-6 AFM images of pure Ni silicideat 700°C

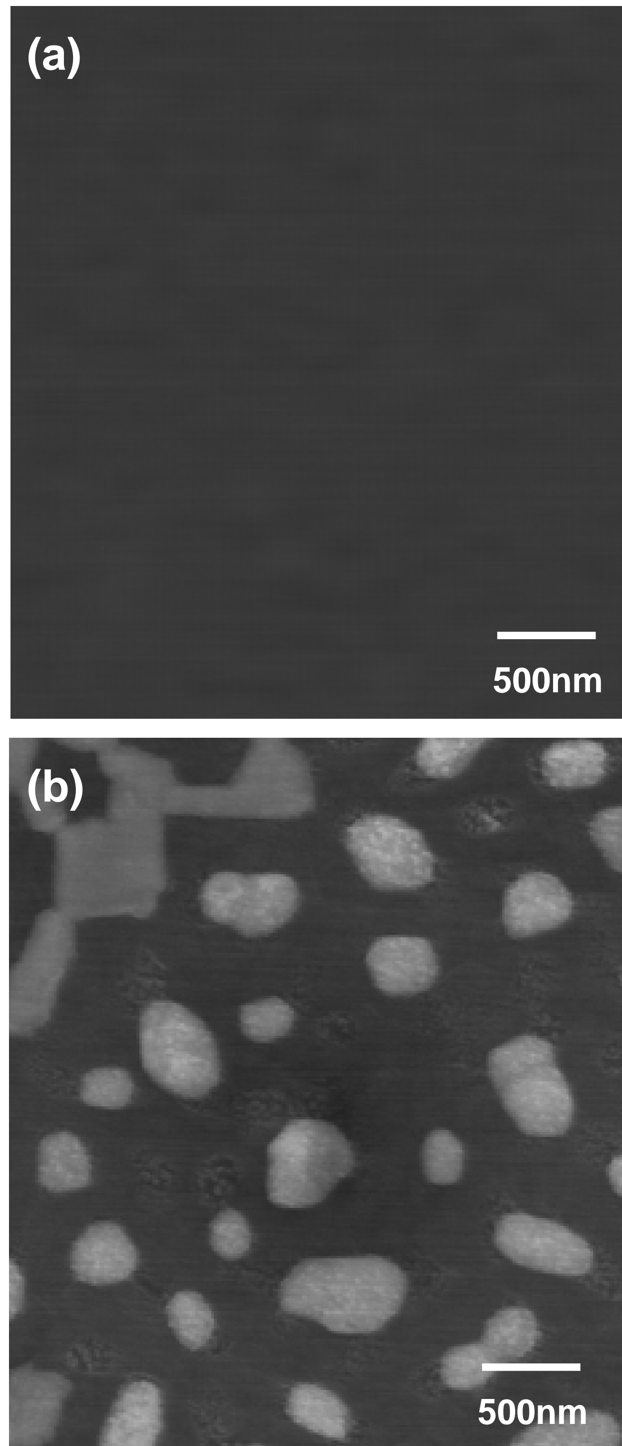

Fig.3-7 SEM images of pure Ni silicides at 600°C (a) and 700°C (b)

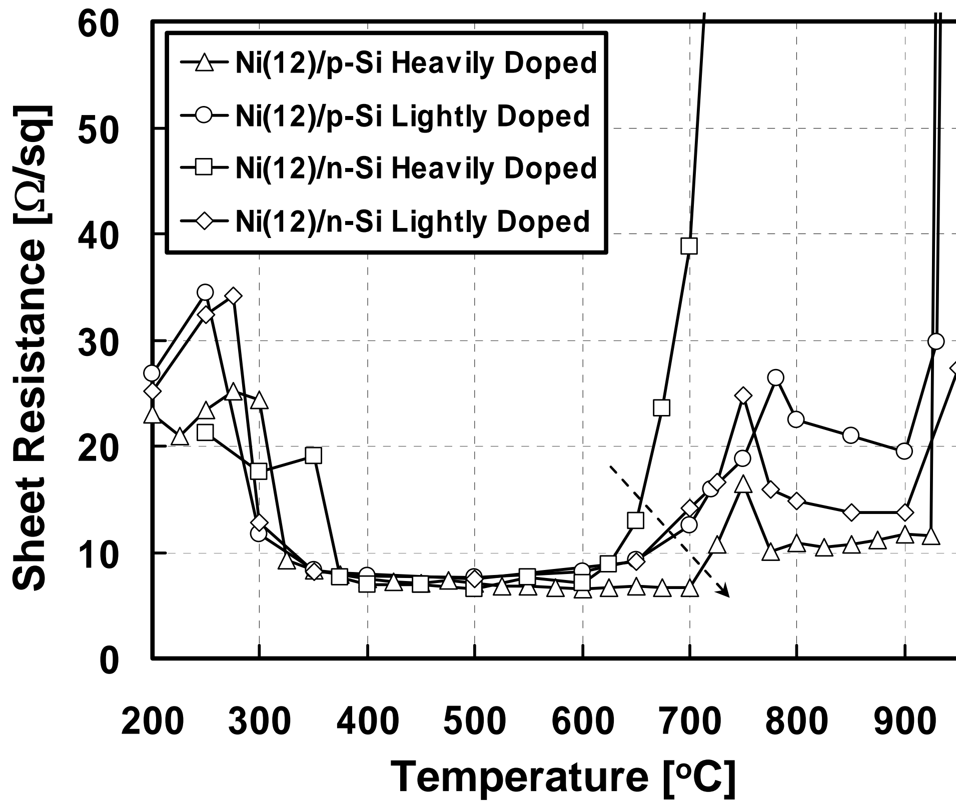

Fig. 3-8 Sheet resistance of dependence on doping concentration

Table.3.1 The details of various substrates

Si Type	ρ (Ωcm)	Doping concentration
N-type (Ion Implantation)	-	$7.5x10^{19}cm^{-3}$
N-type (Bulk)	1.0-1.8	$4x10^{15}cm^{-3}$
P-type (Ion Implantation)	-	$1.5x10^{20}cm^{-3}$
P-type (Bulk)	8-12	$1x10^{15}cm^{-3}$

3.2 Experimental results of Ni silicide with Al layer

As mentioned it in a previous section, it seems that what is nearer to Ni silicide heavily doped p-type Si has better thermal stability. So experiment about Ni silicide with additive of Al which is element of family 3 same as B using dopant of P-type Si was conducted.

3.2.1 Fabrication process of Ni silicide with Al layer

Fabrication process of Ni silicide with Al layer is same as section 3.1.1 except for process of deposition. Ni and thin Al films were deposited *in situ* by sputtering method on heavily doped N^+ (As implanted) or P^+ (B implanted) Si(100) wafers with various layered structures as shown in Fig.3-9. In each structure, thickness of Ni layer was 12 nm (total thickness if Ni was separated to two layers) and Al thickness was 0.6-7.2 nm. In the "Al-near interface" structure, the Ni layers under the Al layer was 0.5 nm, while in the "Al-intermediate" structure, the thickness of Ni layers under and above the Al layer were identical.

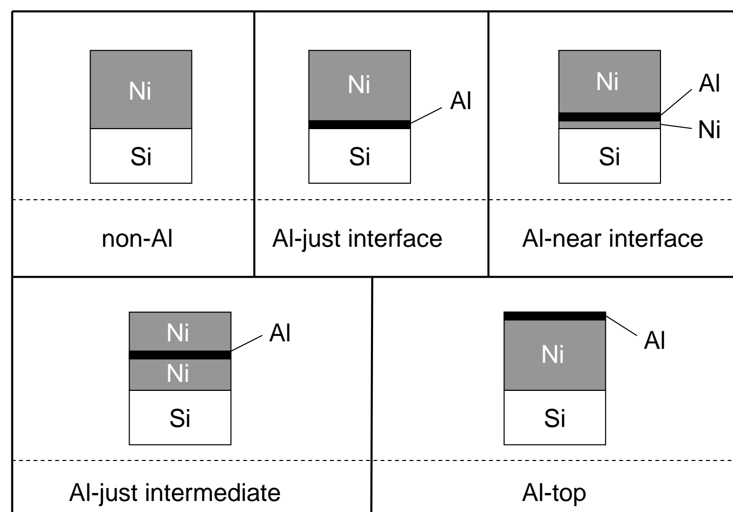

Fig 3-9 Deposited layered structures of Ni and Al before RTA.

3.2.2 Characteristics of Ni silicide with Al layer

In order to overcome the problem of the poor thermal stability on the N^+ substrates, various layered structures as shown in Fig.9 were examined. The transformation curves for the "Al-top", "Al-intermediate" and "Al-near interface" structure with various Al thicknesses on the N^+ substrates are shown in Fig.3-10, Fig.3-11, and Fig.3-12 respectively. The obtained curves for these structures were all close to the reference curve of the "non-Al" structure, indicating no apparent improvement on thermal stability. On the other hand, only the case of "Al-just interface" exhibited obvious improvement of thermal stability on N^+ substrates as shown in Fig.13, in which relatively low sheet resistance was maintained up to 900°C with increasing thickness of the inserted Al layer. Transformation curves for the case of the "Al-just interface" were observed also on the P^+ substrates as shown in Fig.14. The sheet resistances for the case of the "Al-just interface" were low up to higher temperature comparing to the case of "non-Al" structure. In the case of 0.6 nm Al addition, the transformation curve was identical to that of "non-Al", however, the curves became flat for the case of thicker Al addition (3.6 nm and 4.8 nm).

In the case of the "non-Al", significant agglomeration was observed(mentioned it in section 3.1.1), which resulted in the very high sheet resistance. On the other hand, in the case of "Al-just interface", the surfaces were very smooth even at as high as 800°C by surface morphology observed by AFM and SEM shown in Fig.3-15, Fig.3-16, and Fig.3-17. The uniform silicide layers obtained in the wide temperature range is considered to provide rather flat characteristics in the transformation curves as shown in Fig.3-13.

Behavior of the deposited Al was investigated through observation of AES depth

profiles after these silicidation processes. It was fond that almost all Al segregated at the surface after the RTA even if the Al had been deposited under the Ni in the initial stage ("Al-just interface") as shown in Fig.3-19 (a). Furthermore, the Al segregation was observed independent of the initial layered structures of deposition as shown in Fig.3-19 (b), in which Al profiles at the surface are magnified for the cases of 1.2 nm Al deposition in the "Al-just interface", "Al-intermediate" and "Al-top" structures after RTA over 600°C. This means that Ni and Al diffused each other but most of Al was not taken into the formed silicide layers. It should be noticed that the only 0.5 nm separation of Al from the interface, *i.e.*, the "Al-near interface" structure (Fig.9), degraded the effect of thermal stability improvement. It indicates that existence of Al between Ni and Si in the initial stage of silicidation process is essential and Al involvement in the later stage is not so significant.

Structure of the Ni silicide layers were estimated from the AES depth profiles. The averaged composition x of NiSix was evaluated from the relative intensity ratio of Ni and Si in the silicide layer (Fig.3-19 (a)) for each sample. The obtained evaluated compositions were plotted as a function of RTA temperature for the "non-Al" and the "Al-just interface" samples as shown in Fig.3-20 and Fig.3-21. On the N^+ substrates, as shown in Fig.3-20, increase in x with RTA temperature was found to be reduced as thickness of Al increased. The value of x ($1<x<2$) is considered to represent mixture ratio of NiSi(x=1) and $NiSi_2$(x=2). Phase transition from NiSi to $NiSi_2$ occurred entirely for the "non-Al" and the "Al-just interface" with thiner Al (<2.4 nm) in the temperature region of 600-750°C. However, in the case of the "Al-just interface" with thicker Al (>2.4 nm), the increase in x seemed to saturate between 1 and 2. Although it is not clear whether this means coexistence of NiSi domain and $NiSi_2$ domain or formation of

another silicide phase, this situation is possibly related to the suppression of agglomeration at higher temperature region as shown in Fig.3-6 and Fig.3-7 (b). On the P^+ substrates, as shown in Fig.3-21, excessively thick Al layer rather enhanced the phase transition even at 700°C, however, thin Al layer (0.6 nm) did not affect the silicidation characteristics probably since the transformation curve exhibited identical shape to that of original one ("non-Al") as shown in Fig.3-14. Fig.3-18 shows low RTA temperature region of Ni/Si and Ni/Al/Si structure silicide on N^+-Si. Compared to Ni/Si structure, temperature of Ni/Al/Si structure silicide to turn into low resistance phase is lower about 100 °C. As shown Fig.3-2, duration time of RTA is 1 minute and what is changed it to 5 minutes and 30 minutes is plotted in Fig.3-18. Changing the duration time to 30min, the sheet resistance turned to low value.

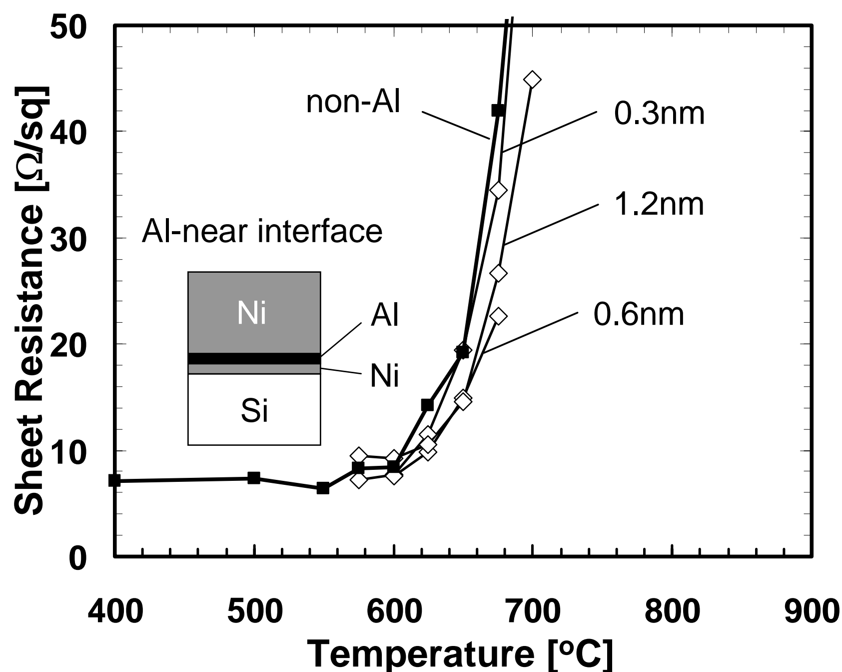

Fig 3-10 Transformation curves for Ni silicide on N^+-Si substrates. Al layer (0.3- 1.2 nm) was inserted at position 0.5nm separated from Ni/Si interface, so called "**Al-near interface**".

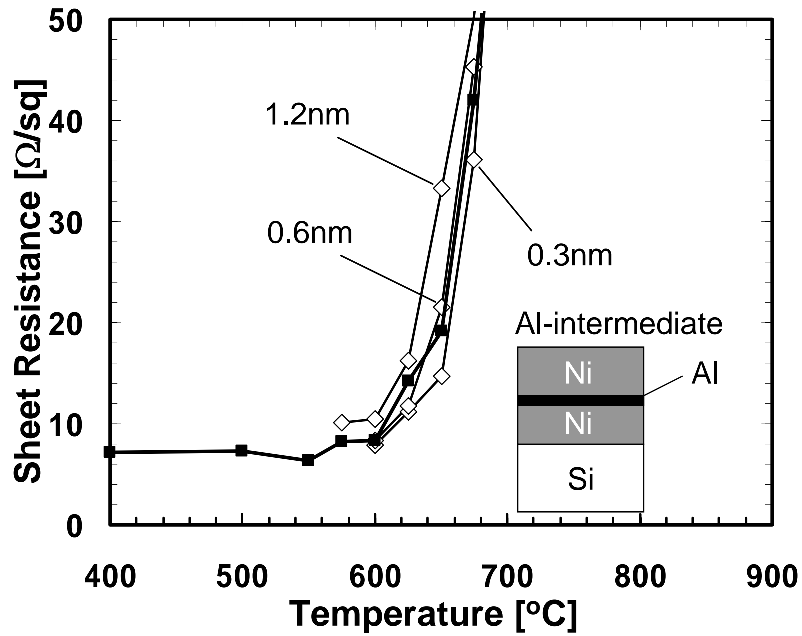

Fig 3-11 Transformation curves for Ni silicide on N^{+}-Si substrates. Al layer (0.3-1.2 nm) was inserted at middle position (top Ni layer: 5nm), so called "**Al intermediate**".

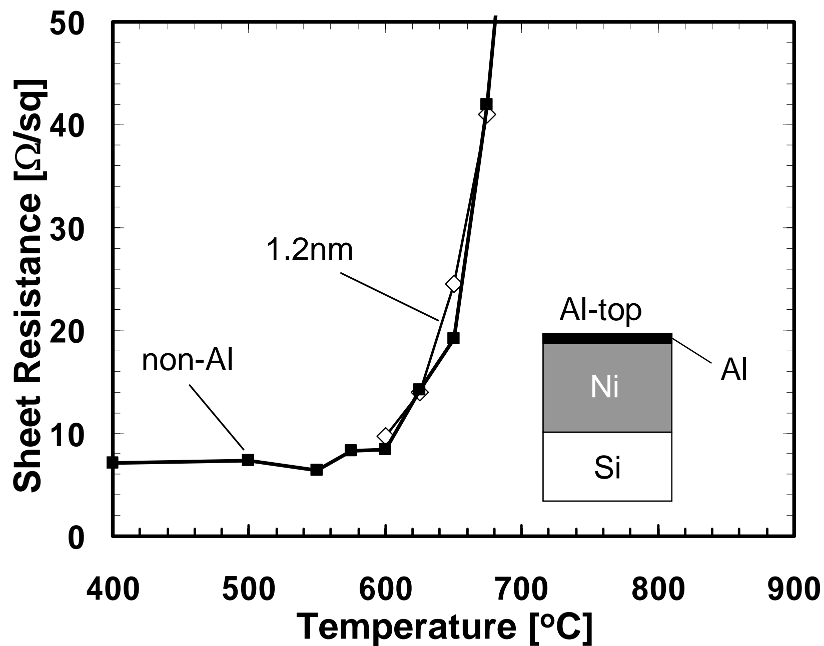

Fig 3-12 Transformation curves for Ni silicide on N^{+}-Si substrates. Al layer (0.3-1.2 nm) was deposited (1.2 nm) on top, so called "**Al-top**"

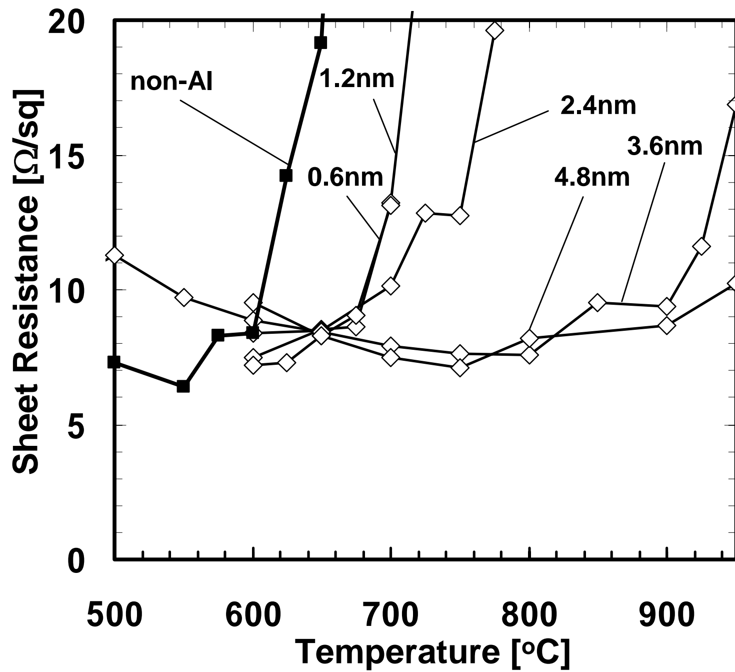

Fig.3-13 Transformation curves for Ni silicide on N^+-Si substrates, formed from "Al-just interface" with 0.6-4.8 nm Al layer, compared with those from "non-Al" reference structure.

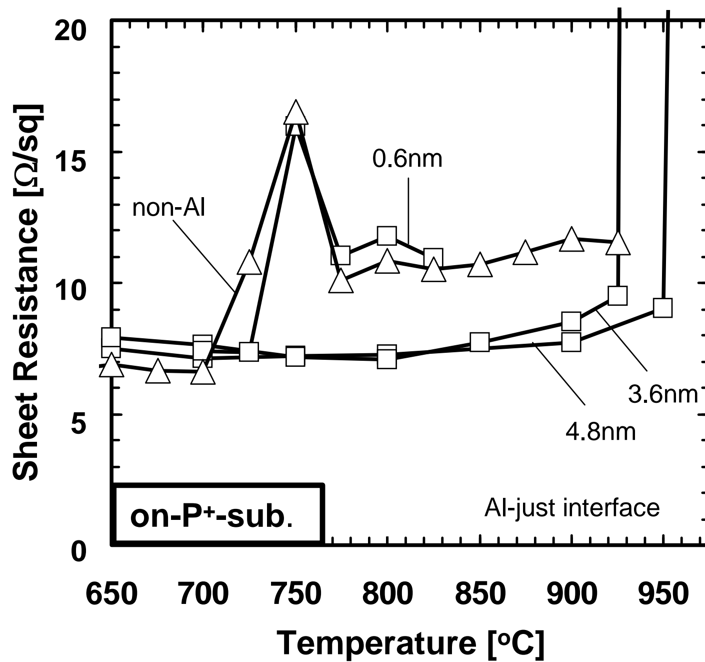

Fig.3-14 Transformation curves for Ni silicide on P^+-Si substrates, formed from "Al-just interface" with 0.6-4.8 nm Al layer, compared with those from "non-Al" reference structure.

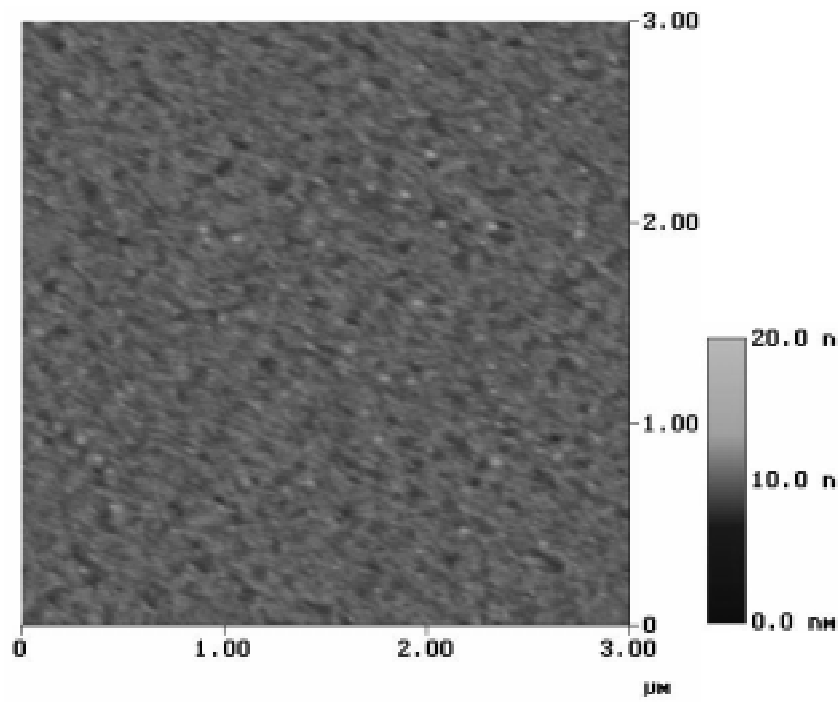

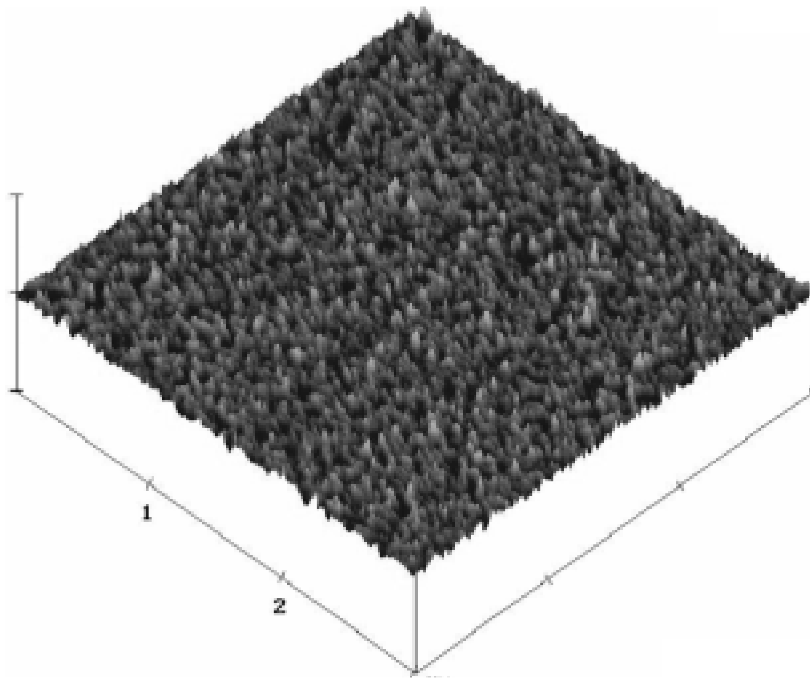

Fig. 3-15 AFM images of Ni/Al/Si structure
(Al just interface) at 600°C

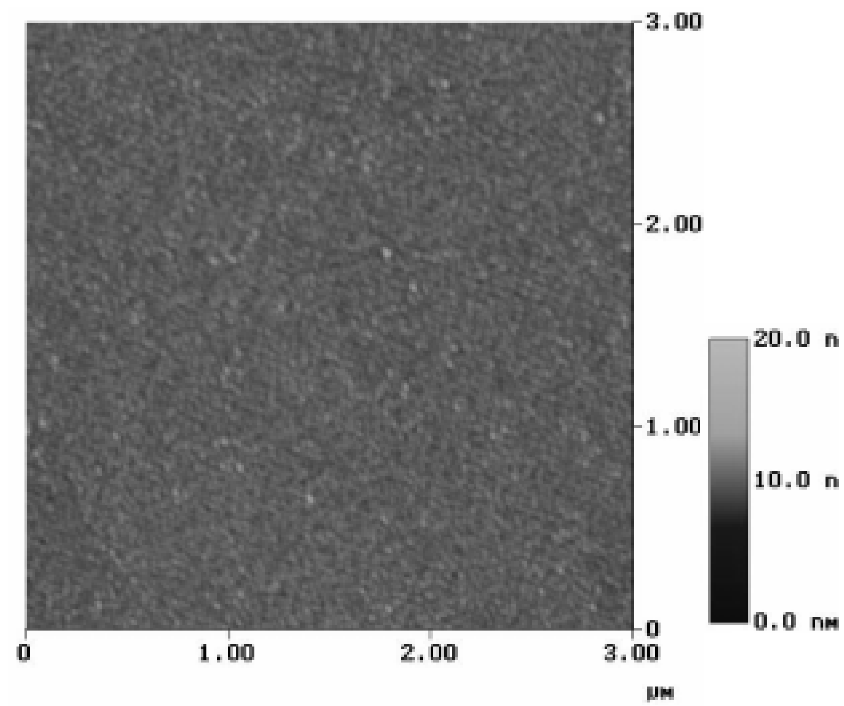

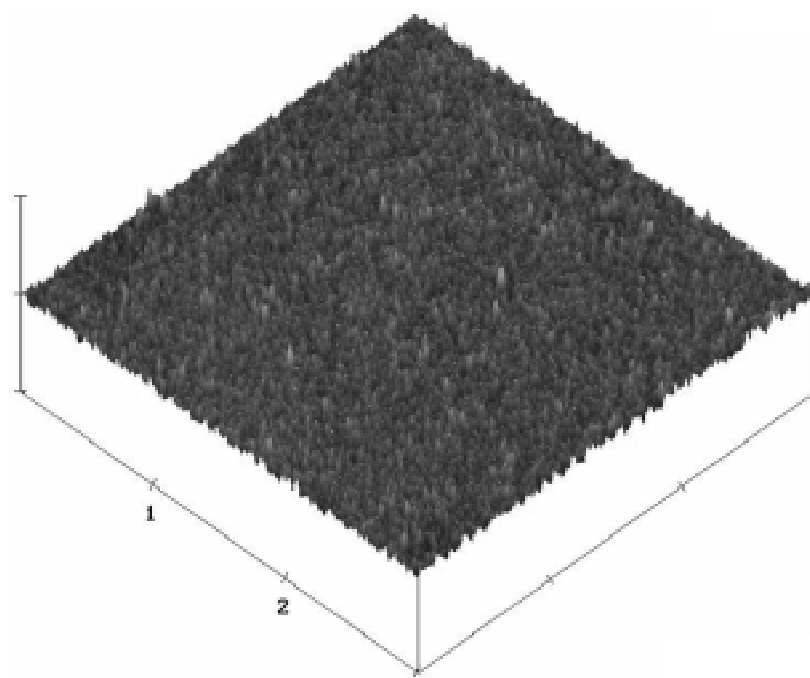

Fig. 3-16 AFM images of Ni/Al/Si structure
("Al just interface") at 700°C

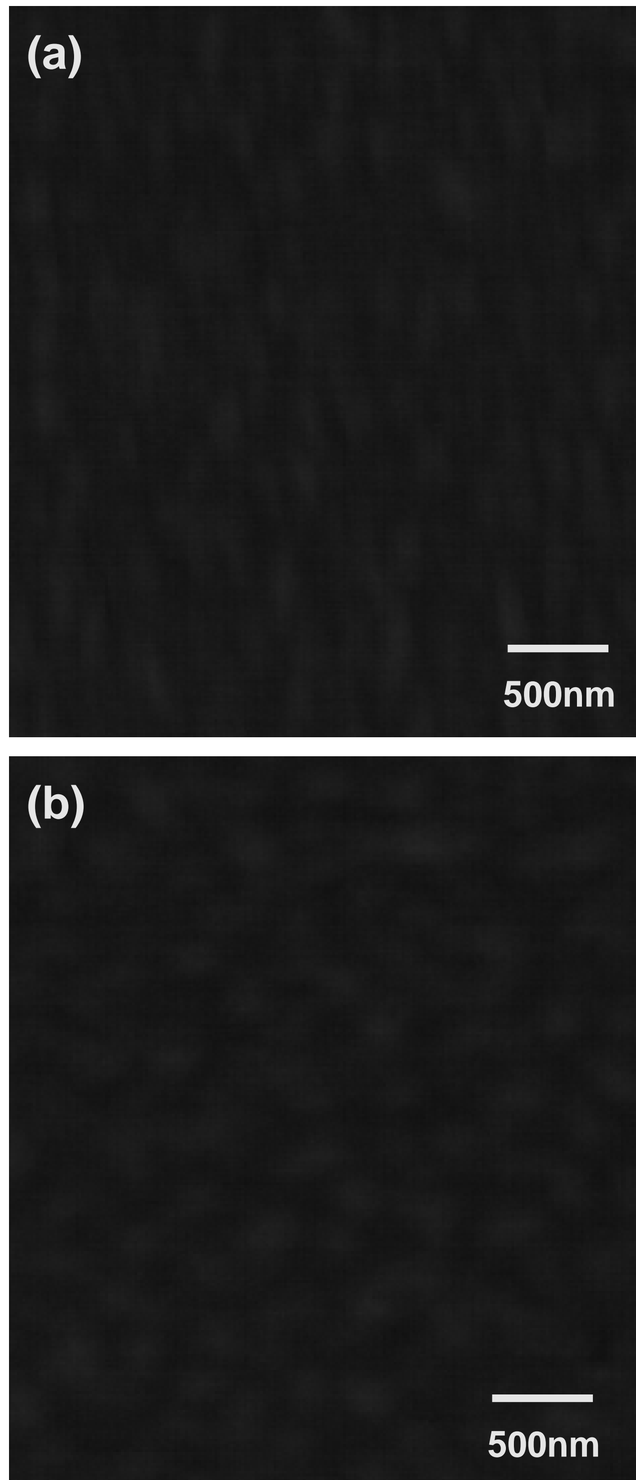

Fig.3.17 SEM images of Ni/Al/Si structure ("Al just interface")
at 600°C (a) and 800°C (b)

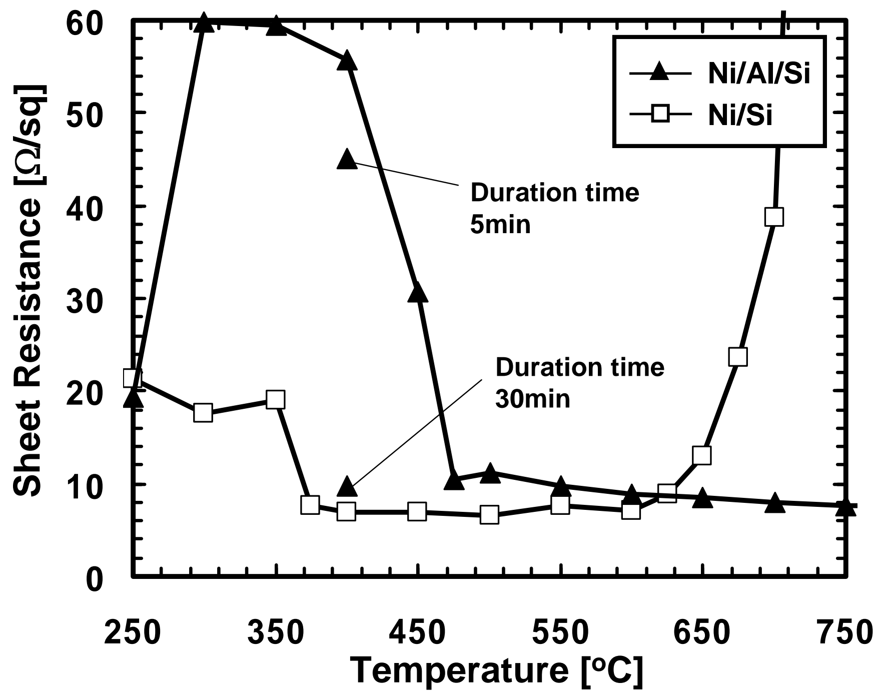

Fig.3-18 Sheet resistance of Ni/Al/Si structure (“Al just interface”) depending on duration time at 400°C. (Al thickness is 3.6nm)

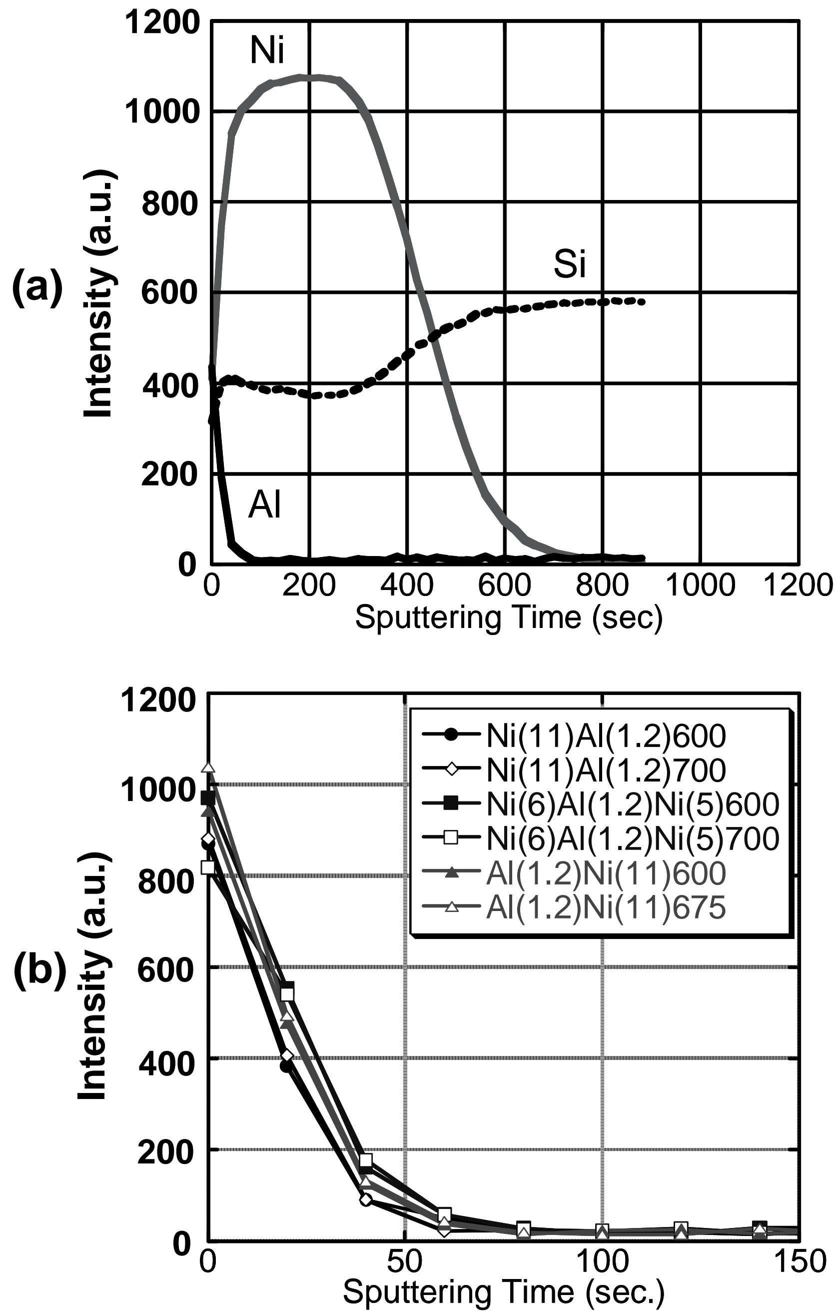

Fig.3-19 (a) AES depth profile for Ni silicide formed from the "Al-just interface" with 1.2 nm Al layer at 600°C. (b) AES depth profiles of Al closed up at the surface for the sample of “Al-just interface”, “Al-intermediate” and “Al-top” with 1.2 nm Al layer annealed at various temperatures. Representation in the legend expresses layer sequence from top to interface, thickness in nm unit, and RTA temperature in °C unit.

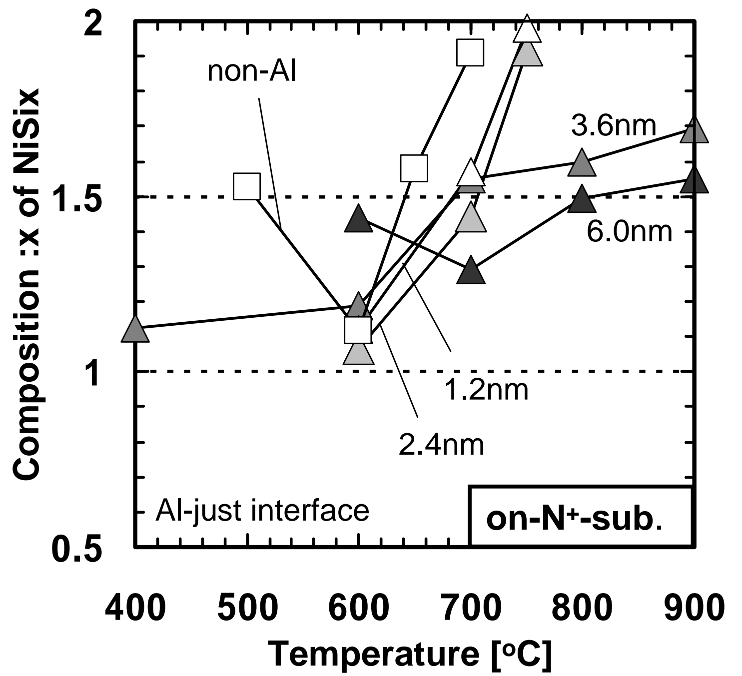

Fig.3.20 Composition, x, of $NiSi_x$ estimated from AES depth profiles as a function of RTA temperature and Al thickness for "non-Al" and "Al-just interface" structures on N^+-Si substrates.

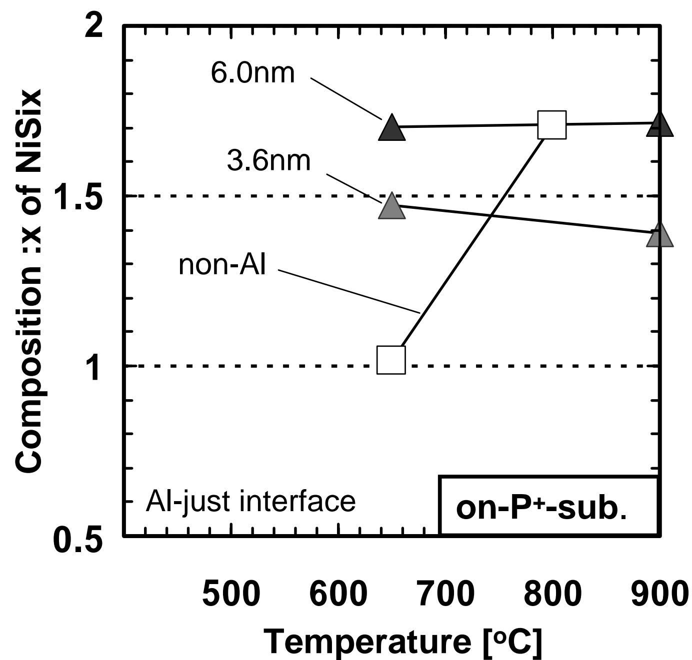

Fig.3.21 Composition, x, of $NiSi_x$ estimated from AES depth profiles as a function of RTA temperature and Al thickness for "non-Al" and "Al-just interface" structures on P^+-Si substrates.

3.3 Experimental results of Ni silicide with Al interlayer using TEG wafer

As mentioned in section 1.3, when the line width is pretty narrow, so called narrow line effect occurs in $TiSi_2$. It is said that the narrow line effect was not observed about Ni silicide, but the property of Ni silicide may be changed by the addition metal. Therefore experimental of Ni silicide with Al interlayer using TEG wafer was conducted.

3.3.1 Fabrication process of Ni silicide with Al layer on TEG wafer

Fabrication process of Ni silicide with Al layer on TEG wafer shown Fig.3-1. Cleaning process was as follows. TEG wafers were dipped into UPW first for 5 minuets. Secondary, they were dipped hydrofluoric acid (HF) for 1 minuets to remove the native oxide. After that, the wafer was rinsed in UPW and loaded to suppurating system immediately. Deposition and Annealing process were performed same as previous section. Finally, the selective etching was carried out to remove non reacted metals.

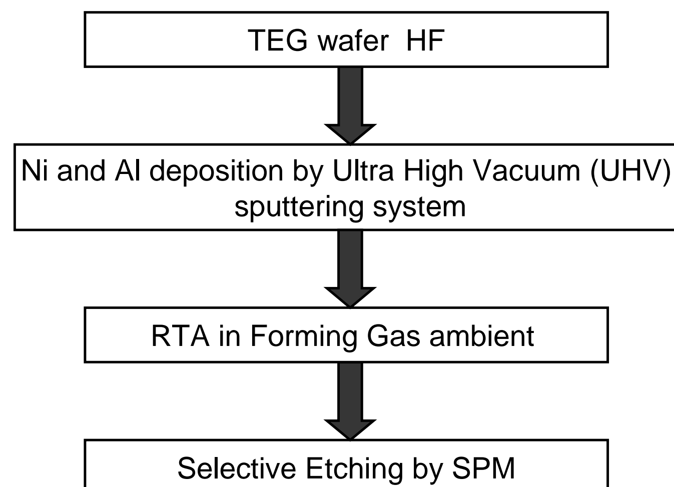

Fig.3-22 Fabrication process of Ni silicide with Al layer on TEG wafer

3.3.2 Characteristics of Ni silicide with Al layer on TEG wafer

Sheet resistances of narrow wire patterns were evaluated as a function of annealing temperature. The two deposition structures with and without 1.2-nm-thick Al layer in the "Al-just interface" were examined. Sheet resistance evaluated on the narrow line patterns (80-1000 nm in width) of P^+ and N^+ diffusion region as a function of RTA temperature, comparing between the deposition structures of Ni only (non-Al) and "Al-just interface" with 1.2nm-Al. Total thickness of deposition was 12nm.

Fig.3-23 shows sheet resistance as a function of line width plotted different RTA temperatures. This graph has 3 axes such as sheet resistance, line width, and RTA temperature. Fig.3-23 was rewired to Fig.3-24 and Fig.3-25 that have 3 axes of X axis, Y axis, and axis of using colors. The axis of color stands for sheet resistance and white means that sheet resistance is under 11.0sq, light gray and dark gray mean that sheet resistance is 11.0 to 20.0 Ω/sq, over 20.0 Ω/sq respectively. For the silicide layers on N^+ diffused regions, the introduction of Al layer was also effective to improve thermal stability. The good thermal stability for P^+ diffused regions for both with and without Al deposition was also consistent with the results on non-patterned substrates. And narrow line effect was not observed both N^+ and P^+ diffused regions for with Al deposition.

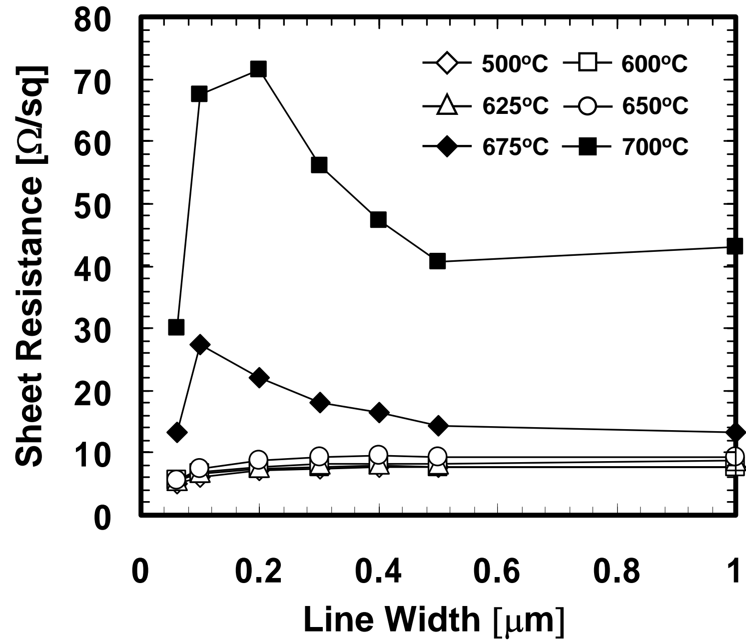

Fig.3-23 Sheet resistance as a function of line width plotted different RTA temperatures

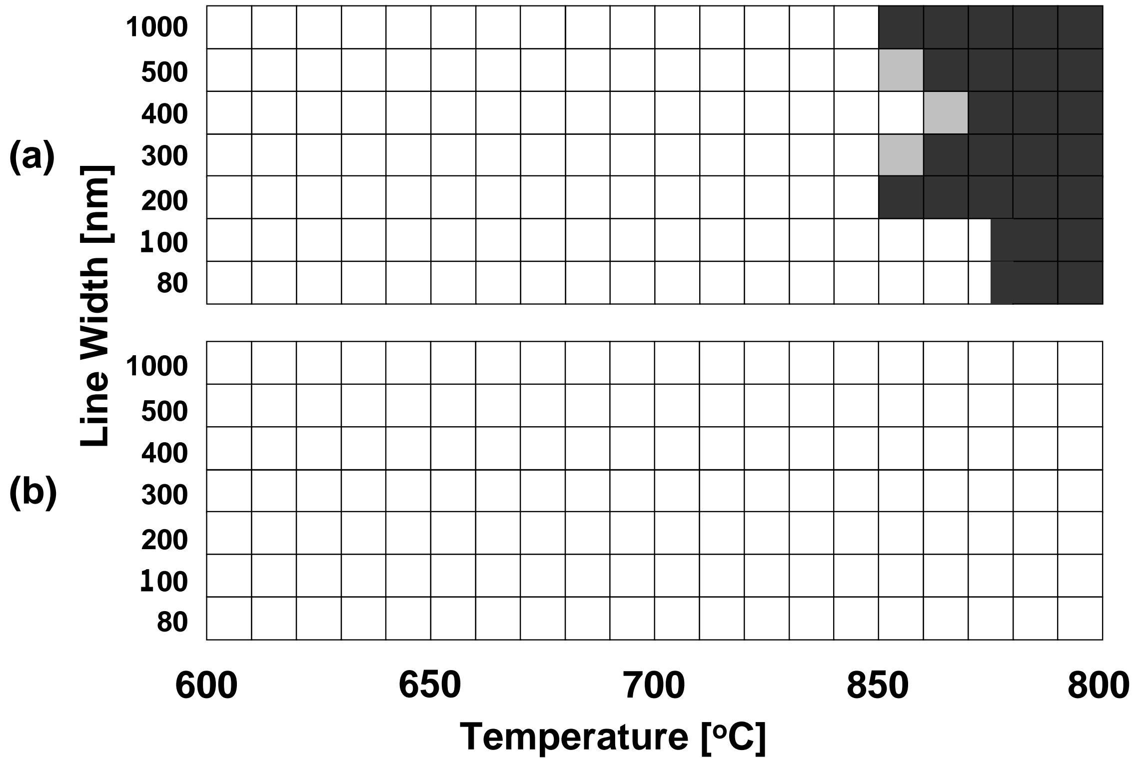

Fig. 3-24 Sheet resistance evaluated on the narrow line patterns (80-1000 nm in width) of P^+ diffusion region as a function of RTA temperature, comparing between the deposition structures of Ni only (non-Al) and "Al-just interface" with 1.2nm-Al. Total thickness of deposition was 12nm.

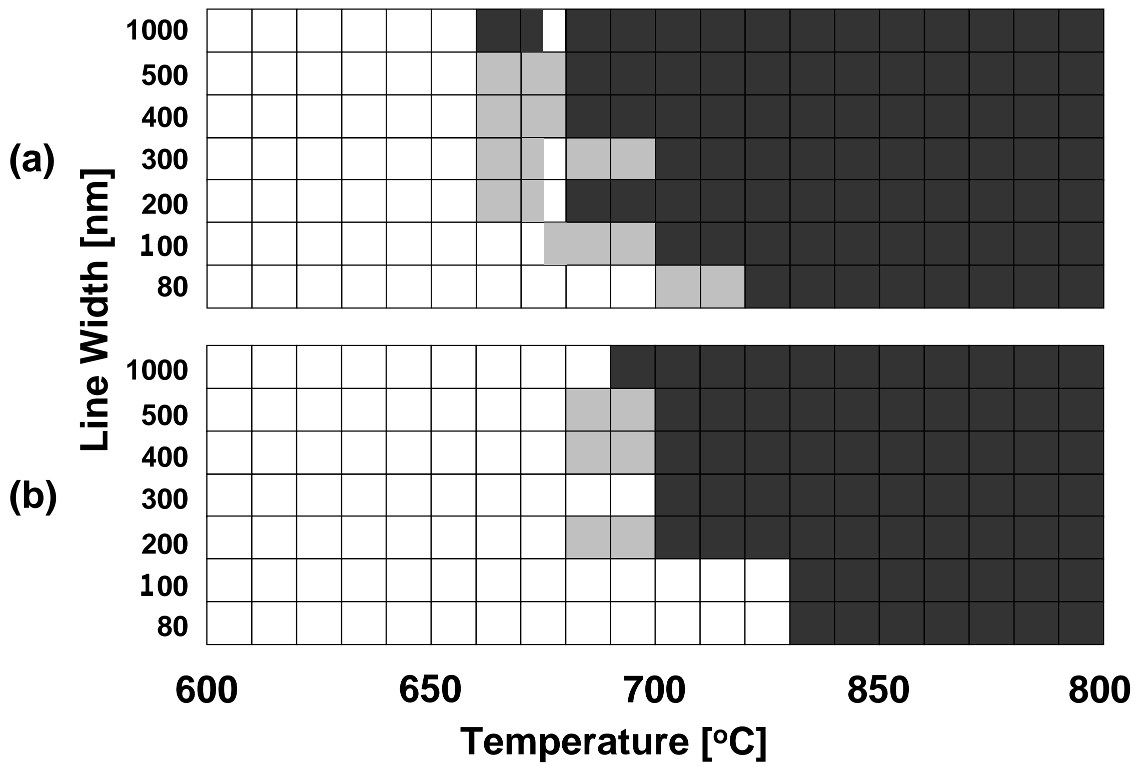

Fig. 3-25 Sheet resistance evaluated on the narrow line patterns (80-1000 nm in width) of N^+ diffusion region as a function of RTA temperature, comparing between the deposition structures of Ni only (non-Al) and "Al-just interface" with 1.2nm-Al. Total thickness of deposition was 12nm.

3.4 Experimental results of Ni silicide with other metal layers

Experiments about Ni silicide with additive of B, Sn, and Pt was conducted. B is element of family 3 same as Al, Sn is element of family 4 same as C which was reported as good element for Ni silicide [6] and Pt was reported a lot for additive metal of Ni silicide [7-15].

3.4.1 Characteristics of Ni silicide with other metal layers

Fig.3.26 shows transformation curves for Ni silicide on N^+-Si substrates, formed from Ni/B/Si with 0.6-3.6 nm B layer, compared with those from Ni/Si (Ni thickness is 12nm). When the B interlayer was 2.4nm, the result was best. And the Silicide degradation temperature rose 75°C. It should be attracted attention that the sheet resistance at starting degradation temperature is as low as pure NiSi.

Fig.3.27 and Fig.3.28 show transformation curves for Ni silicide on N^+-Si substrates, formed from Ni/Sn/Si and Sn/Ni/Si structure with 0.5-1nm Sn layer, compared with those from Ni/Si. Regardless of structure and layer thickness, additions of Sn degraded thermal stability of Ni silicide.

Fig.3-29 and Fig.3-30 shows transformation curves for Ni silicide on N^+-Si substrates, formed from Ni/Pt/Si ,Ni /Pt/Ni/Si(intermediate), and Pt/Ni/Si with 0.6nm and 1.2nm Pt layer respectively, compared with those from Ni/Si.(Ni+Pt thickness was 12nm) Despite of structures, the results were similar but the Pt layer thickness thicker, the sheet resistance was higher. The sheet resistance at starting degradation temperature is higher than pure NiSi unlike B.

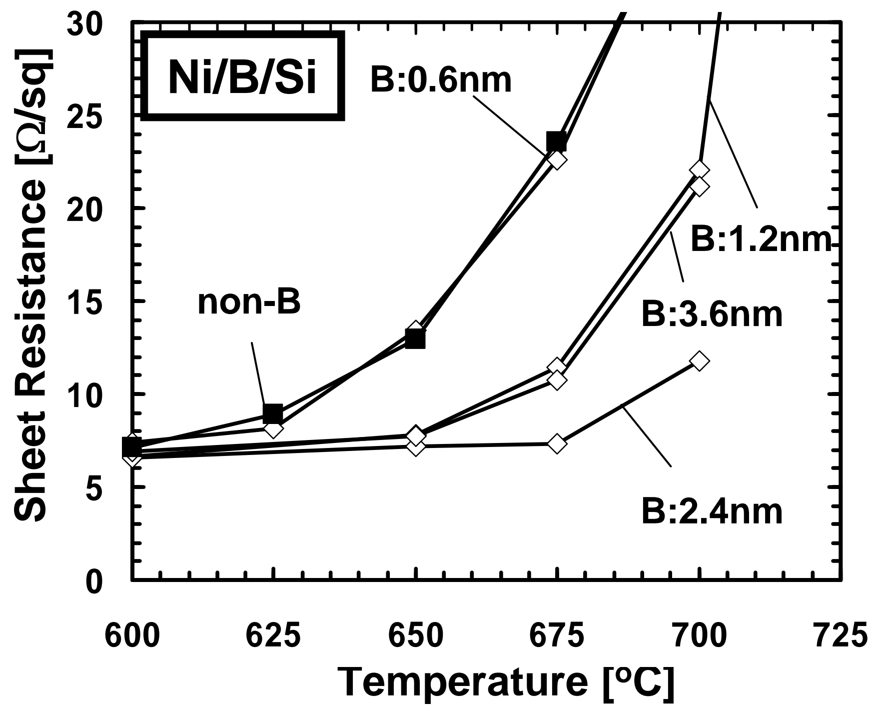

Fig.3.26 Transformation curves for Ni silicide on N^+-Si substrates, formed from Ni/B/Si with 0.6-3.6 nm B layer, compared with those from Ni/Si.

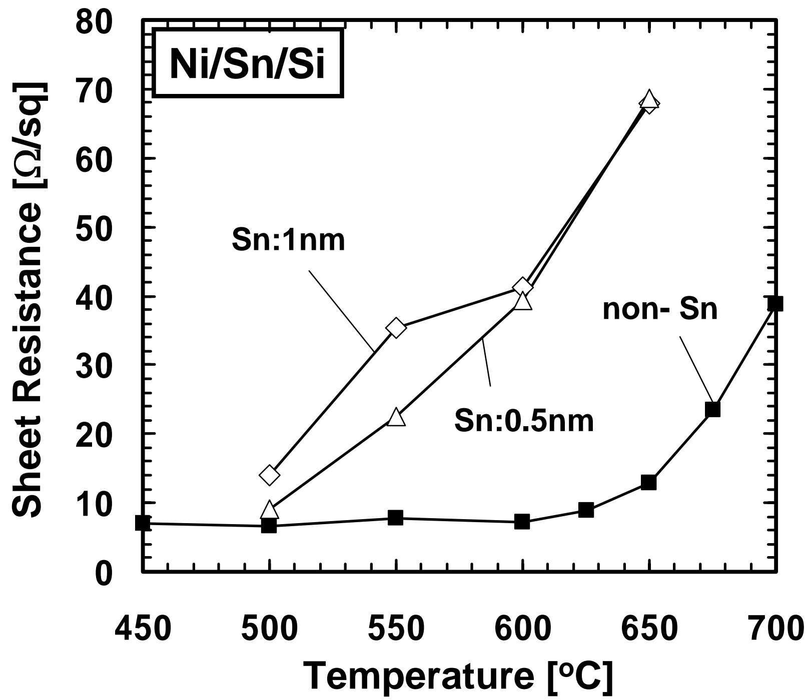

Fig.3.27 Transformation curves for Ni silicide on N^+-Si substrates, formed from Ni/Sn/Si with 0.5 and 1nm Sn layer, compared with those from Ni/Si.

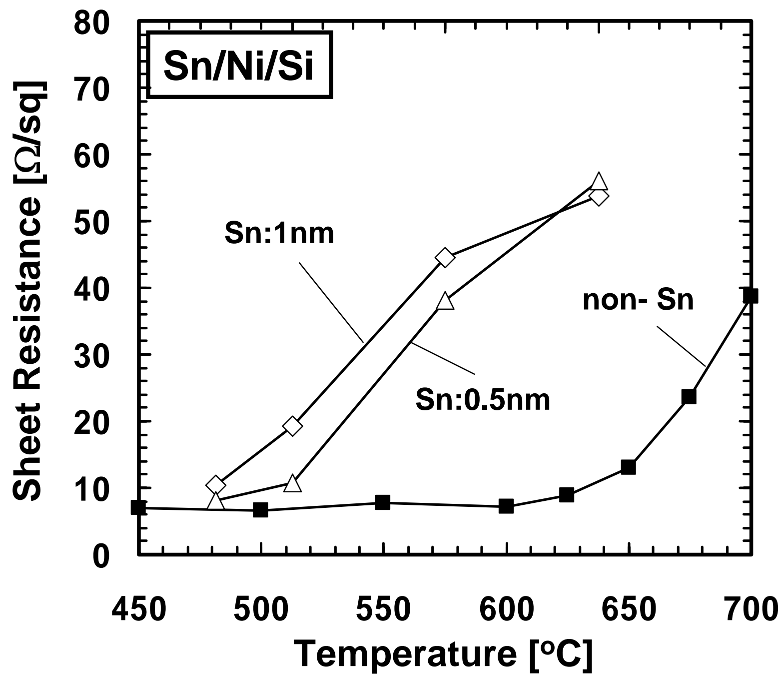

Fig.3.28 Transformation curves for Ni silicide on N^+-Si substrates, formed from Sn/Ni/Si with 0.5 and 1nm Sn layer, compared with those from Ni/Si.

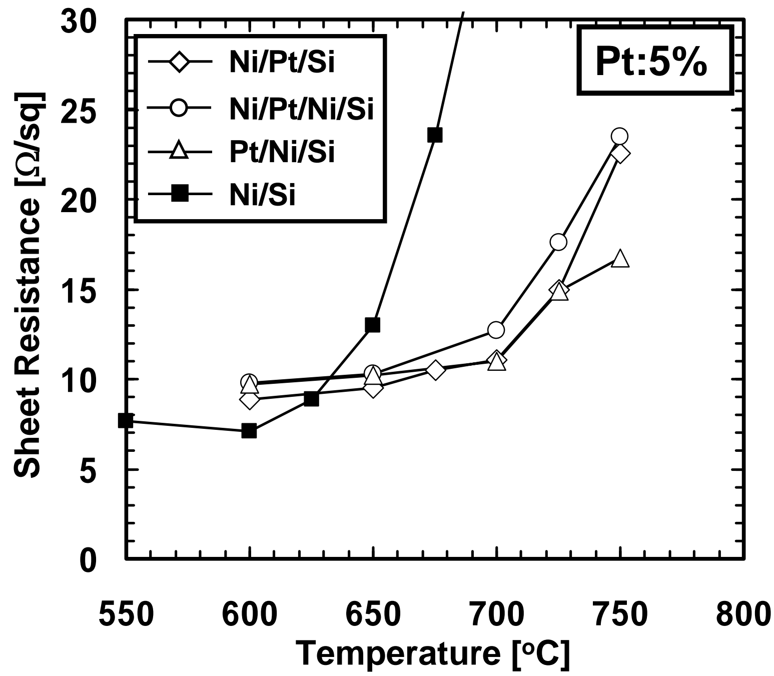

Fig.3.29 Transformation curves for Ni silicide on N^+-Si substrates, formed from Ni/Pt/Si ,Ni /Pt//Ni/Si(intermediate), and Pt/Ni/Si with 0.6 nm Pt layer, compared with those from Ni/Si.

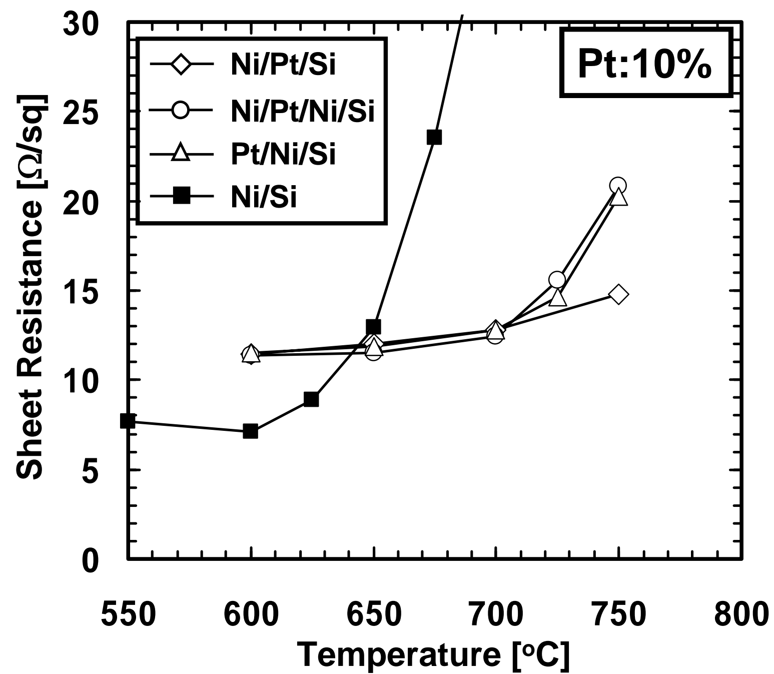

Fig.3.30 Transformation curves for Ni silicide on N^+-Si substrates, formed from Ni/Pt/Si ,Ni /Pt//Ni/Si(intermediate), and Pt/Ni/Si with 1.2 nm Pt layer, compared with those from Ni/Si.

Chapter 4

CONCLUSIONS

4.1 Results of This Study

To begin with, we investigated pure Ni silicide on heavily doped N^+-Si. From it, we found the degrading temperature of Ni silicide on heavily doped N^+-Si was lower about 100°C than that of Ni silicide on heavily doped P^+-Si and the degrading was caused by hard agglomeration.

Secondary, we investigated Ni silicide with Al layer to overcome the problem of the poorer thermal stability on the N^+ substrates, and various layered structures as Al/Ni/Si, Ni/Al/Ni/Si, and Ni/Al/Si were examined. Al/Ni/Si and Ni/Al/Ni/Si structures were not effective to improve the thermal stability of Ni silicide on the N^+ substrates, but the Ni/Al/Si structure was so effective to improve the thermal stability Ni silicide on the N^+ substrates especially Al thickness was over 2.4nm. Sheet resistance of Ni silicide with over 2.4nm Al layer inserting Ni-Si interface maintained under 10Ω/sq up to 900°C which is lower than those of $NiSi_2$ seen on P^+ substrate. And very smooth surface morphologies were observed from SEM and AFM images at 800°C. The same results were observed on P^+ substrate. Composition, x, of $NiSi_x$ estimated from AES depth profiles. As far as the Ni/Al/Si structure (Al thickness: < 2.4nm) is concerned, the increase in x seemed to saturate between 1 and 2. Although it is not clear whether this means coexistence of NiSi domain and $NiSi_2$ domain or formation of another silicide phase, this situation is possibly related to the suppression of agglomeration at higher temperature region. Sheet resistances of narrow wire patterns were evaluated using TEG wafers. And narrow line effect was not observed both N_+ and P_+ diffused regions for with Al (1.2nm) deposition.

Finally, experiments about Ni silicide with additive of B, Sn, and Pt were conducted. We found the Ni silicide on N^+-Si substrates formed from Ni/B/Si with B

layer effective. And the Silicide degradation temperature rose 75°C at the maximum. B is element of family 3 same as Al, therefore we showed possibility that elements of family 3 such as Al and B is effective materials for Ni silicide.

4.2 Future Issues

We showed possibility that elements of family 3 such as Al and B is effective materials for Ni silicide. However the mechanism of its effect is not understood completely. The mechanism should be made clear for applications of silicide for future device. At the same time, a trial to really use this result for real device should be made.

Acknowledgements

I wishes to express his deep gratitude to his supervisor Professor Hiroshi Iwai, who gave him great guidance and support during his Master study. He led me to a treasure of knowledge and showed me what a researcher should be. The experience of doing research in IWAI Lab. was invaluable to me.

I would like to express my sincere appreciation to Associate Professor Kazuo Tsutsui of his very wonderful advices and warm-hearted instructions in my research. He always enlightens my confidence when I have difficulty.

I also want to thank Professor Noriaki Nakayama **for his warmhearted encouragement to make progress in my research.**

I want to express my gratitude to Visiting Professor Takeo Hattori and Visiting Professor Nobuyuki Sugii, who always give me good advices about my research.

I also want to thank Assistant Kuniyuki Kakushima and Assistant Parhat Ahmet for providing an excellent experiment environment and tremendous supports for my research.

I also wants to thank my other silicide group member, Mr. Koji Nagahiro. I want to thank them for their helpful discussions and good cooperation in experiment. I need to thank former silicide group member Xiang Ruifei for providing help in using the experimental tool. Special thanks go to Technical Officer Dai Syoji for teaching me how to carry out SEM measurement.

Many thanks to current and former graduate students, Dr. NG Jin Aun, Dr. Atsushi Kuriyama, Dr. Molina Reyes Joel, Dr. Yuichiro Sasaki, Dr. Hendriansyah Sauddin, Mr. Jaeyeol Song, Mr. Yasuhiro Shiino, Mr. Masayuki Nakagawa, Mr. Kiichi Tachi ,

Manabu Adachi, Yoshihisa Ohisi, Tamasa Kawanago, Soushi Staoh Yasuhiro Morozumi and Ko-ichi Okamoto for many helpful discussions.

I would very much appreciate the great supports from secretaries, Ms. Mikoto Karakawa, Ms. Yuki Hashizume, Ms. Akiko Matsumoto, Ms. Takako Fukuyama, and Ms. Nobuko Iizuka.

This study was supported by ULSI Process Technology Development Center, Semiconductor Company, Matsushita Electric Industrial Co., Ltd. I would like to thank Dr. Yasutoshi Okuno, Mr. Michikazu Matsumoto, and Mr. Masafumi Kubota for their useful advices and indispensable support in Si-substrate supplying and measurements.

Takashi Shiozawa

Yokohama, Japan

January, 2007

References

[1] International Technology Roadmap for Semiconductors (ITRS) 2006 update.

[2] Yuan Taur and Tak H. Ning, "Fundamentals of MODERN VLSI DEVICES" CAMBRIDGE UNIVERSITY PRESS.

[3] H. Iwai, T. Ohguro, and H. Ohmi, "NiSi salicide technology for scaled CMOS" Microelectronic Engineering 60, pp.157-169.

[4] Shi-Li Zhang , Mikael Ostling,*Critical Reviews in Solid State and Materials Sciences,* 28(1):1–129 (2003)

[5] Q. Z. Hong, S. Q. Hong, F. M. d'Heurle, and J. M. E. Harper, "Thermal stability of silicide on polycrystalline Si" *Thin Solid Films* **253**, 479 (1994).

[6] O. Nakatsuka, K. Okubo, A. Sakai, M. Ogawa, Y. Yasuda and S. Zaima, "Improvement in NiSi/Si contact properties with C-implantaition" Microelectronic Engineering 82, pp.479-484 (2005)

[7] J. F. Liu, H. B. Chen, J. Y. Feng and J. Zhu, "Improvement of the thermal stability of NiSi films by using a thin Pt interlayer" Appl. Phys. Lette., 77(14), pp.2177-2179 (2000).

[8] J. F. Liu, J. Y. Feng and J. Zhu, "Comparison of the thermal stability of NiSi films in Ni/Pt/(111)Si and Ni/Pt/(100)Si systems" J. Appl. Phys., 90(2) pp.745-749 (2001)

[9] L. W. Cheng, S. L. Cheng, L. J. Chien, H. C. Chien, H. L. Lee, and F. M. Pan, "Formation of Ni Silicides on (001)Si with a thin interposing Pt layer" J. Vac. Sci. Technol. A, 18(4), pp.1176-1179(2000).

[10] J. Y. Dai, D. Mangelinck, and S.K. Lahiri, Coexistence of hexagonal and orthorhombic structures in NiSi films containing Pt, Appl. Phys. Lette., Vol.75, No.15, 1999, pp.2214-2216.

[11] R.N. Wang, Y. He, J. Y. Feng, Explanation of the enhancement of NiSi thermal stability according to TFD equations and Miedema's model, Nuclear Instruments and Methods in Physics Research, Vol.222, Issues 3-4, 2004 pp.462-468.

[12] P. S. Lee, K. L. Pey, D. Mangelinck, J. Ding, D. Z. Chi, J. Y. Dai, and L.Chane, Phase and Layer Stability of Ni-and Ni(Pt)-Silicides on Narrow Poly-Si Lines, Journal of The Electrochemical Society, 149(6)G331-G335(2002).

[13] P. S. Lee, K. L. Pey, D, Mangelinck, J. Ding, T. Osipowics, and A. See, Layer Inversion of Ni(Pt)Si on Mixed Phase Si Films, Electrochemical and Solid-State Letters, 5(3)G15-G17(2002).

[14] J. F. Liu, J. Y. Feng, and J. Zhu, Film thickness dependence of the NiSi-to-NiSi2 transition temperature in the Ni/Pt/Si(100) system, APPLIED PHYSICS LETTERS Vol.80, No.2,2002,pp.270-272.

[15] C. Detavernier and C. Lavoie, Influence of Pt addition on the texture of NiSi on Si(001), APPLIED PHYSICS LETTERS, Vol.18, 2004pp.3549-3551.